National Library of Canada
Bibliothèque nationale du Canada

Canadian Theses Service
Service des thèses canadiennes

Ottawa, Canada
K1A 0N4

## NOTICE

The quality of this microform is heavily dependent upon the quality of the original thesis submitted for microfilming. Every effort has been made to ensure the highest quality of reproduction possible.

If pages are missing, contact the university which granted the degree.

Some pages may have indistinct print especially if the original pages were typed with a poor typewriter ribbon or if the university sent us an inferior photocopy.

Previously copyrighted materials (journal articles, published tests, etc.) are not filmed.

Reproduction in full or in part of this microform is governed by the Canadian Copyright Act, R.S.C. 1970, c. C-30.

## AVIS

La qualité de cette microforme dépend grandement de la qualité de la thèse soumise au microfilmage. Nous avons tout fait pour assurer une qualité supérieure de reproduction.

S'il manque des pages, veuillez communiquer avec l'université qui a conféré le grade.

La qualité d'impression de certaines pages peut laisser à désirer, surtout si les pages originales ont été dactylographiées à l'aide d'un ruban usé ou si l'université nous a fait parvenir une photocopie de qualité inférieure.

Les documents qui font déjà l'objet d'un droit d'auteur (articles de revue, tests publiés, etc.) ne sont pas microfilmés.

La reproduction, même partielle, de cette microforme est soumise à la Loi canadienne sur le droit d'auteur, SRC 1970, c. C-30.

NL-339 (r. 86/04)

Canada

UNIVERSITY OF ALBERTA

# CMOS CURRENT CONTROLLED OSCILLATORS

©

BY

IVARS GUNAR FINVERS

A THESIS

SUBMITTED TO THE FACULTY OF GRADUATE STUDIES AND RESEARCH

IN PARTIAL FULFILMENT OF THE REQUIREMENTS FOR THE DEGREE

OF MASTER OF SCIENCE

DEPARTMENT OF ELECTRICAL ENGINEERING

EDMONTON, ALBERTA

FALL 1988

Permission has been granted to the National Library of Canada to microfilm this thesis and to lend or sell copies of the film.

The author (copyright owner) has reserved other publication rights, and neither the thesis nor extensive extracts from it may be printed or otherwise reproduced without his/her written permission.

L'autorisation a été accordée à la Bibliothèque nationale du Canada de microfilmer cette thèse et de prêter ou de vendre des exemplaires du film.

L'auteur (titulaire du droit d'auteur) se réserve les autres droits de publication; ni la thèse ni de longs extraits de celle-ci ne doivent être imprimés ou autrement reproduits sans son autorisation écrite.

ISBN 0-315-45606-X

THE UNIVERSITY OF ALBERTA

RELEASE FORM

NAME OF AUTHOR: IVARS GUNAR FINVERS

TITLE OF THESIS: CMOS CURRENT CONTROLLED OSCILLATORS

DEGREE: MASTER OF SCIENCE

YEAR THIS DEGREE GRANTED: 1988

Permission is hereby granted to the UNIVERSITY OF ALBERTA LIBRARY to reproduce single copies of this thesis and to lend or sell such copies for private, scholarly or scientific research purposes only.

The author reserves other publication rights, and neither the thesis nor extensive extracts from it may be printed or otherwise reproduced without the author's written permission.

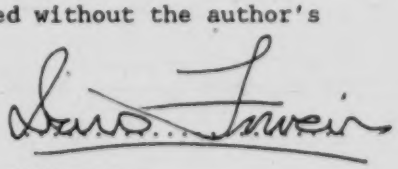

10327 73 Street

Edmonton, Alberta

Canada, T6A 2X3

Date: May 16, 1988

THE UNIVERSITY OF ALBERTA

FACULTY OF GRADUATE STUDIES AND RESEARCH

The undersigned certify that they have read, and recommend to the Faculty of Graduate Studies and Research for acceptance, a thesis entitled CMOS Current Controlled Oscillators submitted by Ivars Gunar Finvers in partial fulfilment of the requirements for the degree of Master of Science

L. D. Lawsky
(Co-Supervisor)

(Co-supervisor)

Date: May 16, 1988

## Abstract

Two CMOS current controlled oscillators, the source coupled and Piskarev multivibrators, are presented. The former utilizes a floating timing capacitor structure and has a combined threshold/current steering circuit, while the latter is based on a grounded capacitor topology and has strict subdivision of the threshold and current steering circuits. For both multivibrators, the frequency versus control current characteristic can be accurately predicted. The determination of the hysteresis voltage of the multivibrator threshold circuit is critical for the frequency calculations. A simple, yet powerful technique is presented for the determination of the hysteresis voltage. First, small signal analysis is applied to the threshold circuit to determine the currents in the threshold transistors at the onset of regenerative switching, then large signal analysis is used to find the hysteresis voltage. The frequency of oscillation then follows quickly. Theoretical calculations are verified experimentally using breadboard techniques (low frequencies) and SPICE simulations (high frequencies). Nonlinearities in the frequency/current control characteristic are present in both multivibrators and the causes are discussed.

**Acknowledgements**

I would like to thank

- my supervisors Igor Filanovsky and Ljubisa Ristic for their advice and encouragement
- the Natural Sciences and Engineering Research Council of Canada and the Alberta Microelelectronics Centre for their financial support
- and Kim for all her encouragement and support.

## Table of Contents


| Chapter | | Page |
|---|---|---|
| 1.0 | Introduction | 1 |
| 1.1 | Applications of current controlled oscillators | 1 |
| 1.2 | CMOS realization | 2 |
| 1.3 | Integration | 3 |
| 1.4 | Multivibrators | 5 |
| 1.5 | Performance Parameters | 7 |
| 1.6 | Thesis Content | 8 |
| 2.0 | Review of current controlled oscillators | 10 |
| 2.1 | CCO topology | 10 |
| 2.2 | CCOs utilizing a floating capacitor topology | 10 |
| 2.2.1 | Emitter coupled multivibrator | 10 |
| 2.2.2 | Wakayama multivibrator | 14 |
| 2.3 | CCOs utilizing a grounded capacitor topology | 17 |
| 2.3.1 | Kukielka multivibrator | 17 |
| 2.3.2 | 4046 type multivibrator | 21 |
| 2.4 | Conclusion | 24 |
| 3.0 | Source coupled multivibrator | 26 |
| 3.1 | Introduction to source coupled multivibrator | 26 |
| 3.2 | Basic operation | 29 |
| 3.3 | Analysis of SCM with no body effect | 34 |
| 3.3.1 | Purely resistive load | 35 |
| 3.3.2 | Combined resistive/active load | 37 |
| 3.3.3 | Purely active load | 38 |
| 3.3.4 | Discussion of results | 39 |

Table of Contents (cont'd)


| Chapter | | | Page |
|---|---|---|---|
| | 3.4 | Analysis of SCM with body effect | 40 |
| | | 3.4.1 Determination of loop gain | 40 |
| | | 3.4.2 Determination of oscillation frequency | 44 |
| | 3.5 | Experimental verification | 51 |
| | | 3.5.1 Experiment 1: purely resistive load | 54 |
| | | 3.5.2 Experiment 2: combined active/resistive load | 57 |
| | 3.6 | Conclusion | 64 |
| 4.0 | Piskarev multivibrator | | 68 |
| | 4.1 | Introduction | 68 |
| | 4.2 | Basic multivibrator | 68 |
| | 4.3 | Threshold circuit | 74 |
| | 4.4 | Complete multivibrator | 78 |
| | 4.5 | Frequency stability | 79 |
| | | 4.5.1 Thermal stability | 80 |
| | | 4.5.2 Jitter | 81 |
| | 4.6 | Choice of hysteresis voltage | 83 |
| | 4.7 | Modification | 83 |
| | | 4.7.1 Buffer | 83 |
| | | 4.7.2 Using buffer output to control charge circuit | 84 |
| | | 4.7.3 Single supply / Split supply operation | 86 |
| | | 4.7.4 Current mirror gain | 88 |
| | | 4.7.5 Voltage gain at input to threshold circuit | 91 |
| | 4.8 | Experimental verification | 91 |

Table of Contents (cont'd)


| Chapter | | | Page |
|---|---|---|---|
| | 4.8.1 | Breadboard verification: experiments 4.1, 4.2a, 4.2b | 93 |
| | 4.8.2 | SPICE simulation: experiments 4.3a, 4.3b, 4.4 | 101 |
| | 4.9 | Discussion | 104 |
| | 4.10 | Conclusion | 108 |
| 5.0 | Review of Results | | 109 |
| | 5.1 | Summary of Results | 109 |
| | 5.2 | Further Research | 110 |
| References | | | 112 |
| List of related papers by author | | | 115 |
| Appendix 1 | | | 116 |
| Appendix 2 | | | 122 |

## List of Tables


| Table | | Page |
|---|---|---|
| 3.1 | Transistor parameters for M1/M2 (NMOS) and M3/M4 (PMOS) for Exp. 3.1 and 3.2 | 55 |
| 3.2 | Circuit parameters for Exp. 3.1, and 3.2 | 55 |
| 4.1 | Typical transistor parameters for Exp 4.1,4.2(a), and 4.2(b) | |
| 4.2 | Circuit parameters for Exp. 4.1,4.2(a), and 4.2(b) | 99 |
| A.1 | Device sizes for CMC.1 | 122 |
| A.2 | Device sizes for CMC.2 | 123 |
| A.3 | Device sizes for CMC.3 | 124 |

## List of Figures


| Figure | | Page |
|---|---|---|
| 1.1 | RC type multivibrator | 4 |
| 1.2 | Constant current type multivibrator | 4 |
| 1.3 | Typical hysteresis characteristic of threshold circuit | 6 |
| 2.1 | Emitter coupled multivibrator | 12 |
| 2.2(a) | Wakayama VCO core | 15 |
| 2.2(b) | Block diagram of VCO | 15 |
| 2.3 | Kukielka multivibrator | 19 |
| 2.4 | 4046 type multivbrator | 22 |
| 3.1(a) | Basic source coupled multivibrator | 27 |
| 3.1(b) | Typical waveforms for source coupled multivibrator | 27 |
| 3.2 | Load configurations (a) resistive load | 30 |
| | (b) active/resistive load | 31 |
| | (c) active load | 32 |
| 3.3 | Small signal equivalent circuit for loop gain calculation | 42 |
| 3.4 | Experimental circuit with purely resistive load | 52 |
| 3.5 | Experimental circuit with combined active/resistive load | 53 |
| 3.6 | Frequency characteristic for the purely resistive load case | 56 |
| 3.7 | Frequency characteristic for the combined active/resistive load case | 58 |
| 3.8 | Variation of $V_{CAP}$ with $\sqrt{I}$ | 60 |

List of Figures (cont'd)


| Figure | | Page |
|---|---|---|
| 3.9 | Variation of $\beta_n$ with $V_{SB}$ | 63 |
| 3.10 | Gate (upper) and source (lower) waveforms for Exp. 3.2 for (a) $I$ = 100 μA and (b) $I$ = 1500 μA | 65 |
| 4.1 | Basic Piskarev multivibrator | 69 |
| 4.1(b) | Typical waveforms for Piskarev Multivibrator | 70 |
| 4.2 | Typical CMOS current switch | 72 |
| 4.3 | Differential pair current switch | 72 |
| 4.4(a) | Small signal equivalent circuit for loop gain calculation | 75 |
| 4.4(b) | Simplified small signal equivalent circuit | 75 |
| 4.5 | Piskarev multivibrator with buffer stage | 85 |
| 4.6 | Piskarev multivibrator with buffer stage controlling charge steering circuit | 87 |
| 4.7 | Threshold setting resistor configuration for single and split supply operation | 89 |
| 4.8 | Gain stage at input of threshold circuit | 92 |
| 4.9 | Threshold circuit | 95 |
| 4.10 | Hysteresis voltage vs. threshold setting resistance | 97 |
| 4.11 | Frequency vs. control current for basic Piskarev multivibrator | 100 |
| 4.12 | Effect of using buffer stage to control the charge steering circuit | 103 |
| 4.13 | Frequency characteristic with extended control range | 105 |

## List of Symbols

| | |
|---|---|
| $A$ | open loop gain |
| $A_{LOOP}$ | closed loop gain |
| $C$ | timing capacitor |
| $CCO$ | current controlled oscillator |
| $CLK+/-$ | clock signal |
| $CMOS$ | complementary metal oxide semiconductor |
| $C_{ox}$ | gate oxide capacitance |
| $ECM$ | emitter coupled multivibrator |
| $FM$ | frequency modulation |
| $f_o$ | oscillation frequency |
| $g_m$ | transistor transconductance |
| $I$ | current |
| $I_C$ | charge current |
| $I_{in}$ | input current |
| $I_{crit}$ | current level at which $f_o \rightarrow \infty$ |
| $I_d$ | transistor drain current |
| $I_T$ | threshold bias current |
| $L$ | length of transistor gate |
| $LC$ | inductor/capacitor network |
| $M(\#)$ | transistor number |
| $m_{th}$ | threshold parameter |
| $NMOS$ | n-channel MOSFET |
| $PLL$ | phase lock loop |
| $PMOS$ | p-channel MOSFET |
| $Q$ ($\bar{Q}$) | output signal of SR (set/reset) flipflop |

## List of Symbols (cont'd)

| | |
|---|---|
| $R$ | resistor |
| $R_{bias}$ | bias current setting resistor |
| $RC$ | resistor/capacitor network |
| $R_{eq}$ | ac equivalent of the threshold setting resistor |
| $r_o$ | ac equivalent of output resistance of a current source |
| $SCM$ | source coupled multivibrator |
| $SPICE$ | circuit simulation program |
| $SR$ | set/reset flipflop |
| $T$ | period (total) |
| $TC$ | temperature coefficient |
| $T_o$ | period (ideal - no switching delays) |
| $T_{SD}$ | switching delays |
| $V_C$ | voltage across the timing capacitor |
| $V_{CAP}$ | voltage across the timing capacitor at instant of transition |
| $VCO$ | voltage controlled oscillator |
| $V_{CC}$ | positive supply voltage |
| $V_d$ | voltage at drain of transistor |
| $V_{gs}$ | voltage across the gate source of a transistor |
| $V_H$ | upper threshold voltage |
| $V_{HYST}$ | hysteresis voltage |
| $V_L$ | lower threshold voltage |
| $V_{ref}$ | reference voltage |
| $V_S$ | voltage at the source of transistor |
| $V_T$ | thermal voltage ($kT/q$) |
| $V_{tn,p}$ | threshold voltage of NMOS and PMOS FETs with body effect |

## List of Symbols (cont'd)

| | |
|---|---|
| $V_{tno,po}$ | threshold voltage of NMOS and PMOS FETs without body effect |
| $W$ | width of MOSFETs gate |
| $Z$ | generalized load impedance |
| $\beta$ | gain coefficient of MOSFET ($\mu\ C_{ox}\ W/L\ /\ (1+\delta)\ /\ 2$) |
| $\beta_{nT}$ | gain coefficient of threshold devices |
| $\beta_{nC}$ | gain coefficient of charge steering devices |
| $\delta$ | correction factor for $\beta$ |
| $\gamma$ | body effect coefficient |
| $\phi_f$ | Fermi voltage |
| $\square$ | square - area measure for integrated resitors |

## 1.0 Introduction

### 1.1 Applications of Current Controlled Oscillators

Current controlled oscillators (CCO) are a useful and versatile electronic building block. A CCO can be used directly for the generation of clock signals for timing applications, and for the generation of carrier signals which can be modulated in amplitude and frequency to facilitate the transmission of information. Other, more complex systems such as frequency synthesizers, tone decoders, and phase lock loops (PLL) [1] use the CCO as a key element. In the PLL a voltage controlled oscillator (VCO) is used; a VCO can be formed by the combination of a CCO with a voltage to current converter. The PLL is an extremely useful device; among its many applications are AM and FM demodulation, clock recovery, carrier synchronization, and signal conditioning [1]. The CCO can also be combined with a counter/timer to form a simple and inexpensive (albeit slow) analog to digital converter [5]. CCOs have also found application in the area of integrated silicon sensors [2,3,4], providing conversion of the sensor's output signal (typically a voltage or current) into a frequency signal, to improve noise immunity during transmission and to allow the multiplexing of many sensor outputs onto a single transmission line.

The CCO is rarely used as a single entity; usually it is only one element of a larger system. However, the performance of the overall system is often strongly infuenced by the characteristics of the CCO. Consider, for example, the PLL. The VCO is the critical block in a PLL, determining the stability of the center frequency, distortion in

FM demodulation applications, high frequency capability and, possibly, the tracking range [1,9].

## 1.2 CMOS Realization

The trend in electronics is towards integration of entire systems onto a single chip to reduce size and cost, yet provide increased performance [6,7,8]. This can mean the integration of both analog and digital circuitry on a single chip. The analog circuitry provides the interface to the real (analog) world while the digital circuitry, with its high degree of flexibility, provides the majority of the signal processing. In most mixed analog/digital integrated circuits the digital circuitry constitutes the bulk of the circuitry and as a result the fabrication technology is usually optimized for digital applications. For many applications, CMOS is the technology of choice for digital circuitry due to its high packing density, low power consumption, scalability, and availability of design tools [6]. For analog circuits, however, bipolar technology is often more suitable due to the superior performance of bipolar transistors in terms of input noise, offset, voltage gain, output drive, and maximum frequency in comparision to the MOSFET [6]. As a result, the development of monolithic CCOs (and analog circuits in general) in CMOS has not advanced as far as in bipolar. Until the advent of mixed analog/digital chips the need for CMOS CCOs was not very large and the bipolar versions were often preferred.

## 1.3 Integration

The need to integrate CCOs in CMOS places restrictions on the types of oscillators which can be used. Oscillators based on frequency selective networks [9] such as LC networks, quartz crystals, or RC networks (which require close absolute tolerances) are not very suitable due to their limited tuning range and the unavailability of these components in CMOS. The cost of adding these components externally is often prohibitive and defeats the purpose of integration.

A class of oscillators suitable for integration and frequency control are the multivibrator or relaxation oscillator [9]. Throughout this text the terms current controlled oscillator, multivibrator, and relaxation oscillator will be used interchangeably. The frequency of self-sustained oscillation in a multivibrator is set by the time required to charge/discharge a capacitor between two thresholds. Two major classes of multivibrators exist: RC and constant current. In the RC type (Fig. 1.1(a)) the timing capacitor is charged/discharged through a resistance, this results in an exponential form for the capacitor waveform (Fig. 1.1(b)). The timing capacitor of the constant current type multivibrator (Fig. 1.2(a)) is charged/discharged by a constant current which results in a linear waveform (triangular) for the voltage across the capacitor (Fig. 1.2(b)). For CCO applications, the constant current type multivibrator is more suitable since tuning can be achieved via the charge current, whereas for the RC type the resistive/capacitive component must be altered. A typical constant current multivibrator

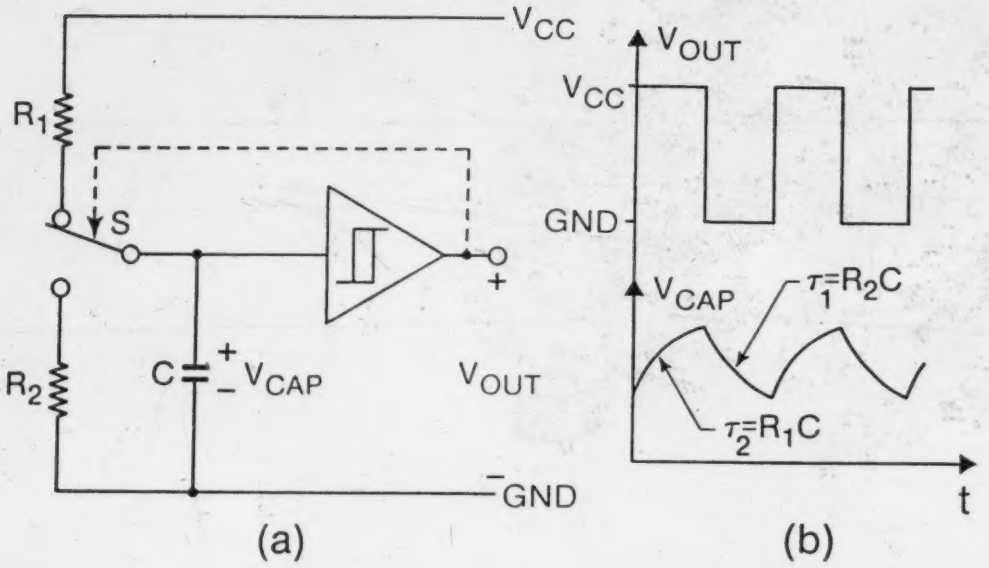


Figure 1.1 RC Type Multivibrator

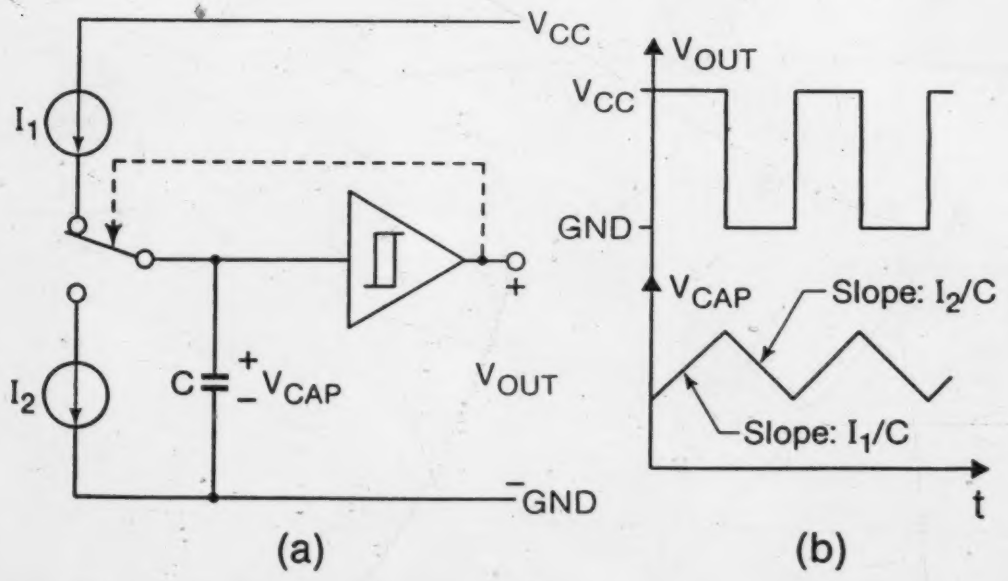


Figure 1.2 Constant Current Type Multivibrator

consists of current sources, switches, a capacitor, and a threshold/control circuit. All these elements are easily fabricated in standard CMOS technology.

## 1.4 Multivibrators

The most important portion of a multivibrator is the threshold/control circuit. This circuitry senses when the voltage across the capacitor has reached a threshold point and then causes the capacitor charging current to reverse. The transfer characteristic of the threshold circuit (Fig. 1.3) is bistable in form and resembles that of a Schmitt trigger. Many of the performance parameters of the multivibrator such as the linearity, range, and stability of operation are directly dependent upon the performance of the threshold circuit.

Consider the simplified schematic of the multivibrator shown in Fig. 1.2(a) and assume that, initially, the capacitor is discharged and the output of the threshold circuit is low. The current source is connected to the capacitor and charges it linearly with a constant current $I$ towards the upper threshold. Once the threshold point is reached the threshold circuit undergoes regenerative switching and the output goes high. The current sink is now connected to the capacitor and it discharges linearly towards the lower threshold, at which point the threshold circuit undergoes regenerative switching forcing the output low. The charge/discharge cycle repeats and the circuit enters astable operation.

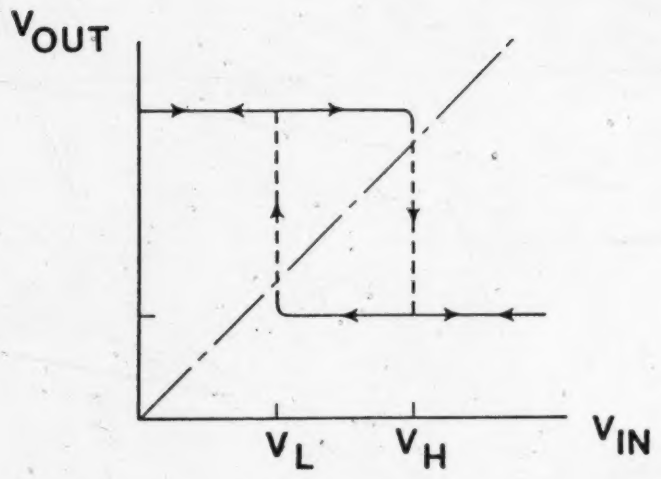


Figure 1.3 Typical Hysteresis Characteristic of Threshold Circuit

The time required for the capacitor to charge between the two thresholds is given by

$$\frac{T}{2} = \frac{\left[ V_H - V_L \right] C}{I} = \frac{V_{HYST}\ C}{I} \qquad (1.1)$$

where $V_H$ = upper threshold

$V_L$ = lower threshold

$V_{HYST} = V_H - V_L$ = hysteresis voltage

$I = I_1 = I_2$ = charge/discharge current

$C$ = timing capacitor

$T$ = period of oscillation

The overall frequency of oscillation is given by

$$f_o = \frac{1}{T} = \frac{I}{2\ C\ V_{HYST}} \qquad (1.2)$$

Linear control of the frequency can be achieved by the variation of the charge/discharge current $I$.

## 1.5 Performance Parameters

A CCO should possess the basic qualities: good stability of the frequency with noise, variations in temperature, and power supply voltage; good linearity and range of frequency control with current; high frequency operation; economical use of chip area; and suitability for operation at the low supply voltages of digital circuitry. The stability, linearity, and high frequency capability affect the amount

of information that can be encoded onto a signal for a given bandwidth, and the supply voltage and area consumption influence the cost and ease of integration.

## 1.6 Thesis Content

This thesis investigates two CMOS CCOs: the source coupled and Piskarev multivibrators. The source coupled multivibrator is the CMOS equivalent of a popular bipolar CCO, the emitter coupled multivibrator. No work on, or use of, the source coupled multivibrator has appeared in literature, therefore an investigation was carried out to determine if the CMOS equivalent is capable of the excellent performance which the bipolar version displays in terms of linearity, range of frequency control, and simplicity. The Piskarev multivibrator is a new design which makes use of separate current steering/threshold circuitry to achieve linear frequency control.

Two major current controlled multivibrator topologies are discussed in Chapter 2 and four representative circuits in both bipolar and CMOS technology are presented. This review suggests that futher investigation into CMOS CCOs is required in both topologies. The first topology, based on the floating timing capacitor, is investigated with the source coupled multivibrator in chapter 3. Due to the highly nonlinear nature of multivibrators, calculation of the exact frequency of oscillation is difficult. A simple, yet powerful technique for determining the transition point of quasistable circuits is presented in Chapter 3. The technique is then applied to the threshold circuits of both the source coupled and Piskarev

multivibrators to determine the frequency of oscillation. Chapter 4 presents the work on the Piskarev multivibrator, which is representative of the grounded capacitor topology.

## 2.0 Review of Current Controlled Oscillators

### 2.1 CCO Topology

Topologically, current controlled multivibrators can be divided into two major groups: floating and grounded timing capacitor. In bipolar technology both topologies are well represented by such circuits as the Cordell emitter coupled CCO [10] (floating capacitor) and the Kukielka CCO [11] (grounded capacitor). In CMOS technology only very recently has appeared a CCO based on a floating capacitor topology [12]. In general, CMOS CCOs have been based on a grounded capacitor structure [9,13,14,15]. A brief overview of four CCOs representative of the two major topologies in both bipolar and CMOS technology will be presented. The advantages and disadvantages of the various structures will be discussed and from this two CMOS multivibrators worthy of further investigation will be suggested.

### 2.2 CCOs Utilizing a Floating Capacitor Topology

#### 2.2.1 Emitter Coupled Multivibrator

The bipolar emitter coupled multivibrator (ECM) is based on the floating capacitor topology and possesses wide dynamic range, good linearity, high frequency capability, and simplicity. A variety of CCOs based on the ECM can be found in literature [10,16,17]; the primary differences between these designs are the methods of temperature compensation used. Voltage controlled oscillators (VCOs) based on the ECM have found wide application in circuits such as PLLs. A monolithic VCO is usually a CCO combined with a voltage to current converter; the terms VCO and CCO will be used interchangeably

throughout this text.

The operation of the classic ECM (without temperature compensation), shown in Fig. 2.1, will now be discussed. The ECM is bistable in nature; the cross coupling of M1 and M2 ensures that either M1 or M2 is ON but not both. In this way the current $I$ is steered through the timing capacitor $C$ from left to right (M1 is ON) or from right to left (M2 is ON). After initial power up of the circuit the voltage across C is zero and due to noise either M1 or M2 will be ON. Consider that M1 is ON and M2 OFF. A current of $2I$ flows through M1 and M5 and no current flows through M2 and M6. Transistors M3 and M4 simply provide buffering and level shifting for M1 and M2 (current sources $I_a$ provide biasing for M3 and M4). The voltage at the emitter of M1 is held fixed at two diode drops ($2V_{BE,ON}$) below $V_{CC}$. The emitter voltage of M2 decreases with a slope of $I/C$ until it is three diode drops below $V_{CC}$ at which point M2 begins to turn ON. The increase of current through M2 causes the base voltage of M1 to decrease, turning M1 further OFF and this in turn causes M2 to turn futher ON. The cross coupling of M1 and M2 provides positive feedback; once the loop gain of this feedback exceeds +1 regenerative switching occurs turning M1 OFF and M2 ON (or vice versa for the opposite transition). Now the emitter voltage of M2 is held at two diode drops below $V_{CC}$ and the emitter voltage of M1 jumps by one diode drop above this (since the voltage across the capacitor at the point of switching was one diode drop and cannot change instantaneously). The emitter voltage of M1 decreases linearly with a slope of $I/C$ until it is three diode drops below $V_{CC}$ at which point the circuit begins to

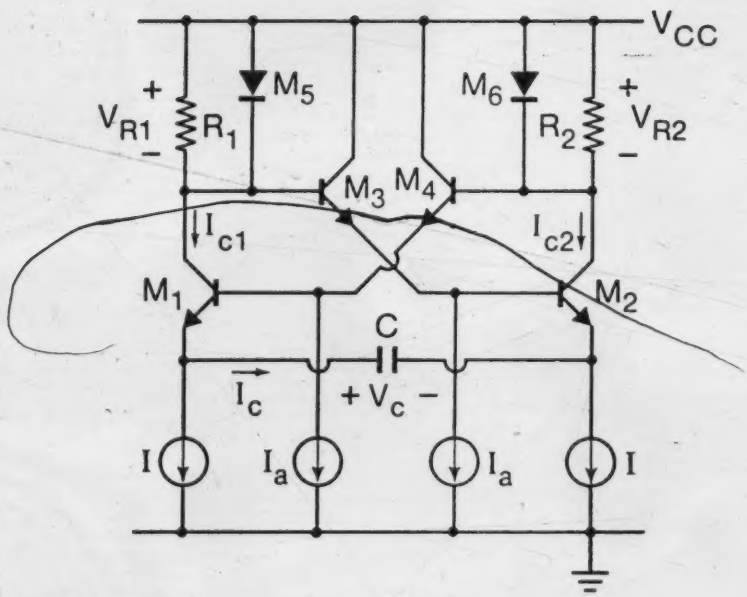


Figure 2.1 Emitter Coupled Multivibrator

switch again. One cycle is now complete and the circuit enters astable operation. Between switching points the voltage across the capacitor changes by two diode drops ($2V_{BE,ON}$) and is charged by a current of $I$, therefore the time for half a cycle (1/2 period) is

$$\frac{T}{2} = \frac{2\,C\,V_{BE,ON}}{I} \qquad (2.1)$$

From which the frequency of oscillation can be found to be

$$f_o = \frac{1}{T}\,\frac{I}{4\,C\,V_{BE,ON}} \qquad (2.2)$$

To the first order $V_{BE,ON}$ can be considered to be independent of current, therefore linear control of frequency can be obtained through the parameter $I$.

The temperature coefficient of the base emitter voltage is approximately -2 mV/°C which causes the frequency to have a temperature coefficient of approximately (for $V_{BE,ON} = 0.6$ V)

$$\frac{1}{f_o}\,\frac{df_o}{dT} = -\,\frac{1}{V_{BE,ON}}\,\frac{dV_{BE,ON}}{dT} \approx 3300 \text{ ppm/°C} \qquad (2.3)$$

A variety of approaches have been taken to reduce this large temperature coefficient. Cordell [10], for example, has constructed a circuit with a temperature coefficient of ± 20 ppm/°C (at 1 kHz) and a maximum operating frequency in excess of 20MHz. Gilbert [16] developed an EMC based multivibrator with slightly higher temperature coefficient (±30 ppm/°C) but the circuit has a very wide range of frequency control, in excess of 10,000:1.

The emitter coupled multivibrator's all-NPN construction,

nonsaturated operation, and small signal swings combine to produce a CCO capable of high frequency operation with good linearity over a wide range. Temperature compensation circuitry is required, though, to improve the inherently poor temperature stability of the basic EMC.

### 2.2.2 Wakayama Multivibrator

Most CMOS CCOs found in the literature are based on grounded capacitor topology. Very recently Wakayama [12] proposed a CMOS VCO which uses a floating capacitor topology. The Wakayama multivibrator shows good frequency capability ( > 30 MHz ), good linearity ( 0.02% over the range of 1 → 15 MHz ), low jitter ( < 100 ppm ), and a temperature coefficient of 340 ppm/°C.

The core of the Wakayama VCO is shown in Fig. 2.2(a) and the overall block diagram of the VCO is found in Fig. 2.2(b). The core is formed primarily by two NMOS FETs (M1, M2) connected as a differential pair and two vertical npn transistors (M3, M4). The bipolar transistors are formed by the source/drain diffusion (emitter), p-well (base), and substrate (collector, tied to $V_{CC}$) and can be fabricated in any standard p-well CMOS technology. To understand the operation of the core, first consider that *CLK+* is high ($V_{CC}$) and *CLK-* is low (*GND*); this forces M1, M4 to be *ON* and M2, M3 to be *OFF*. The emitter voltage of M4 (*Vramp+*) is held at one diode drop below $V_{CC}$ and the drain voltage of M1 (*Vramp-*) ramps downward with a slope of $I_{in}/C$ until the voltage across *C* (sensed at *Vramp+* and *Vramp-*) is equal to the threshold of the SR (set/reset) flipflop (see Fig. 2.2(b)). Once the threshold voltage is exceeded the flipflop changes states and *CLK+*

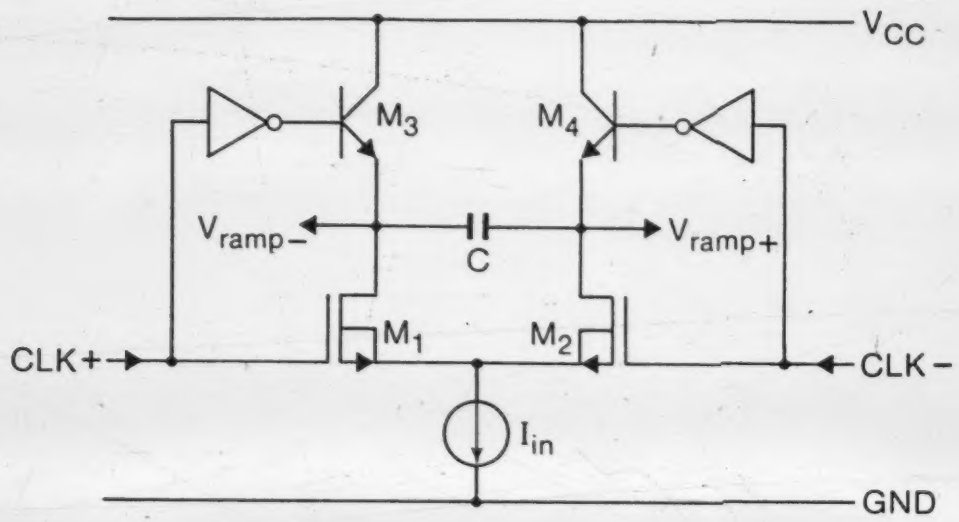


Figure 2.2(a) Wakayama VCO Core

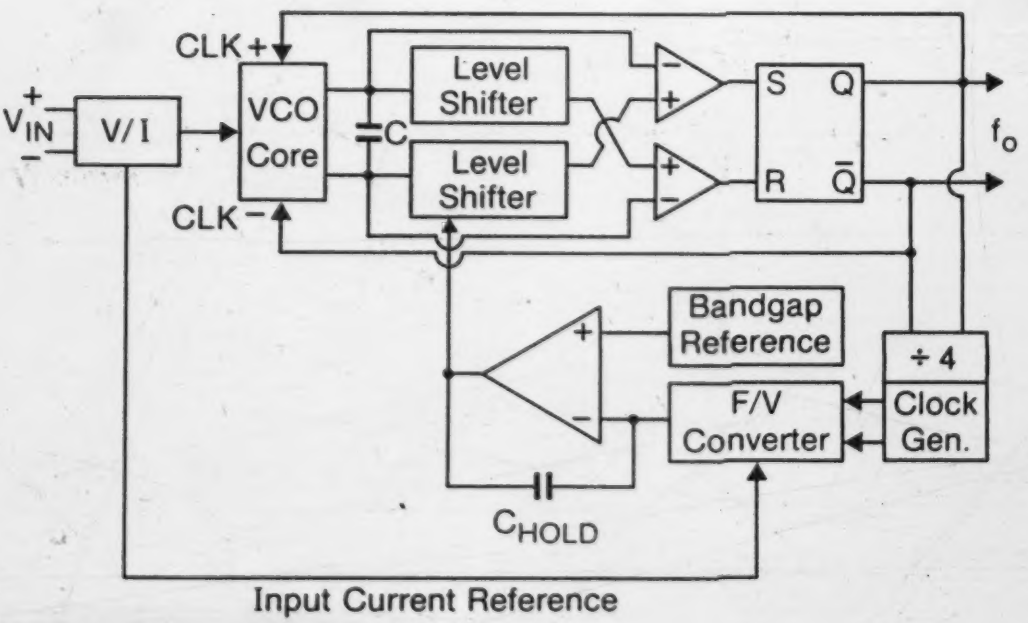


Figure 2.2(b) Block Diagram of VCO

goes low and *CLK-* goes high forcing M2, M3 *ON* and M1, M4 *OFF*. The emitter voltage of M3 is now held at one diode drop below $V_{CC}$ and the voltage at the drain of M2 swings above $V_{CC}$ by an amount equal to $V_{threshold} - V_{BE,ON}$, where $V_{threshold}$ is the voltage across the capacitor at the instant the flipflop undergoes regenerative switching. The drain voltage of M2 then ramps down with a slope of $I_{in}/C$ until the voltage across the capacitor exceeds the threshold of the SR flipflop at which point *CLK+* goes high and *CLK-* goes low. One cycle is now complete and the circuit enters astable operation. A key feature of the Wakayama design is the use of the NPN devices (M3, M4) which allow the swing of the unconstrained end of the capacitor to exceed $V_{CC}$ due to the current blocking provided by the reverse biased base emitter junction of the *OFF* device. This allows the voltage swing of the capacitor to be made large, in this case equal to $V_{CC}$, improving jitter performance [18].

The threshold circuit (Fig. 2.2(b)) is comprised of an SR flipflop, two comparators, and two level shifters. In the actual implementaion the comparators and flipflop are combined to achieve faster switching. The threshold voltage is set by the amount of level shift and the total amplitude of the triangular waveform of the voltage across the timing capacitor is equal to twice the level shift.

A frequency to voltage feedback loop is used to linearize the frequency characteristic [19]. A switched capacitor technique generates a control voltage proportional to the integral of the difference between the input current $I_{in}$ and a current proportional to the output frequency. The control voltage is then used to vary the

amount of level shifting provided by the level shifters (and, therefore, altering the threshold voltage) so that the amplitude of the capacitor's triangular waveform remains constant, independent of frequency. For example, if switching delays result in the amplitude of the triangle wave increasing, the feedback loop reduces the threshold voltage in such a manner as to bring the amplitude back to a reference level. This method reduced the nonlinearity from > 2 % without feedback to less then 0.02 % with feedback.

The Wakayama multivibrator has two primary features: large voltage swings for the capacitor to reduce jitter, and frequency feedback to improve linearity. The multivibrator was fabricated in 3$\mu$ technology and is capable of operation at frequencies in excess of 30 MHz. The one disadvantage of the Wakayama multivibrator is the circuit complexity and resulting area consumption (104 mils x 154 mils).

## 2.3 CCOs Utilizing a Grounded Capacitor Topology

### 2.3.1 Kukielka Multivibrator

A major problem of the emitter coupled based multivibrators is temperature stability. As mentioned before, various approaches have been used to provide temperature compensation. Unfortunately, as the frequency increases, temperature stability is reduced. For example, the Cordell multivibrator has a $\pm$ 20 ppm/$^{\circ}$C TC (temperature coefficient) at 1 kHz but at 1 MHz this has increased to over $\pm$400 ppm/$^{\circ}$C and increases rapidly thereafter. The poor high frequency TC is primarily caused by the parasitic and junction capacitance (with

strong temperature coefficients) that appear at both of the emitters (M1, M2 of Fig. 2.1) which are connected to the timing capacitor. These capacitances form a voltage divider with the timing capacitor and limit the high frequency performance [10,11]. To improve the high frequency temperature stability Kukielka [11] has chosen a grounded capacitor multivibrator topology. The parasitic capacitances now appear in parallel with the timing capacitor and no longer strongly affect high frequency operation. The Kukielka multivibrator achieves a temperature coefficient of < 60 ppm/°C for frequencies up to 20 MHz. One price paid for the improved high frequency temperature coefficient is a reduction in linearity (<3 %) over this range of frequency.

The Kukielka multivibrator (Fig. 2.3) uses separate threshold and current steering circuits. The threshold circuit, consisting of a Schmitt trigger (a comparator with hysteresis), senses the voltage across the capacitor and when the threshold voltage is reached the output changes state and the current switch reverses the direction of the capacitor charging current. The Schmitt trigger is formed by the differential pair M1, M2 with resistive loads $R_{L1}$ and $R_{L2}$, while M5 provides positive feedback to obtain a comparator with hysteresis. The current switch is constructed by using M3, M4 in a differential pair configuration. Level shifting is provided by M6, and M7 with diodes D1 → D3 included to avoid saturation at high temperatures.

After application of power the capacitor $C$ is discharged, this forces M2 and M5 to be *ON* and M1 and M4 to be *OFF*. The capacitor charges up linearly with a slope of $I_o/C$ until the threshold of the Schmitt trigger is reached, at which point M1 and M2 change states and

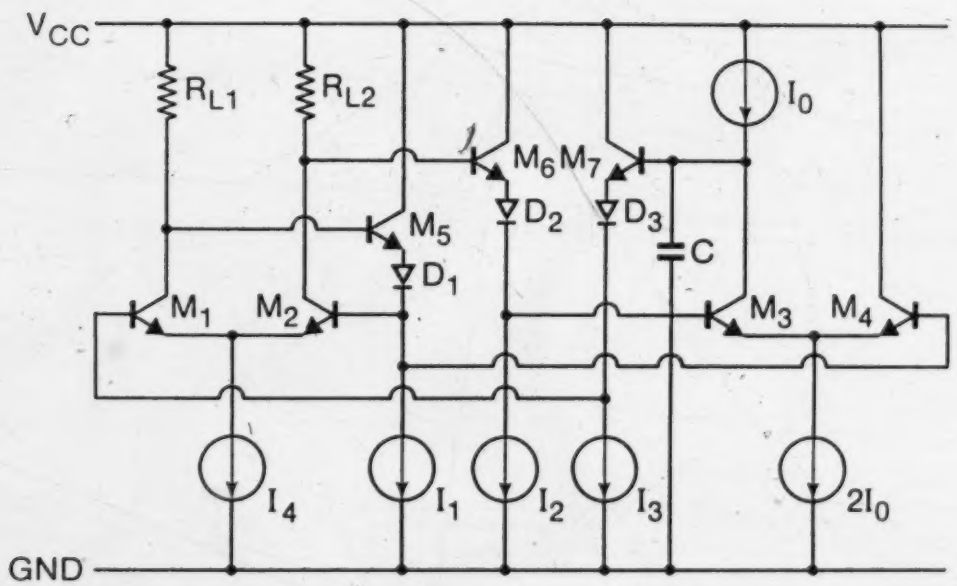


Figure 2.3 Kukielka Multivibrator

M4 turns *ON* discharging the capacitor with a difference current of $2I_o - I_o = I_o$. The capacitor discharges linearly until the lower threshold is reached at which point M1 → M4 all change states and the cycle repeats. From [11] the frequency of oscillation is found to be

$$f_o = \frac{I_o}{2\,C\,V_{HYST}} \tag{2.4}$$

where

$$V_{HYST} = I_4 R_{L1} \cdot \frac{2\,I_4\,R_{L1}}{\frac{I_4 R_{L1}}{2V_T} + \sqrt{\left[\frac{I_4 R_{L1}}{2V_T} - 1\right]^2 - 1}} \cdots$$

$$- 2V_T \ln\left\{\left[\frac{I_4 R_{L1}}{2V_T} - 1\right] + \sqrt{\left[\frac{I_4 R_{L1}}{2V_T} - 1\right]^2 - 1}\right\} \tag{2.5}$$

(assuming $R_{L1} = R_{L2}$). From (2.4) it can be seen that temperature compensation can be achieved by making

$$I_4 R_{L1} = k_1 V_T \tag{2.6}$$

and

$$I_o = k_3 V_T \tag{2.7}$$

where $k_1$ and $k_3$ are constants (see [11]), then

$$f_o = \frac{k_3}{2\,C\,k_4} \tag{2.8}$$

with

$$k_4 = k_1 - \frac{2\,k_1}{\frac{k_1}{2} + \sqrt{\left[\frac{k_1}{2} - 1\right]^2 - 1}} - 2\ln\left\{\frac{k_1}{2} - 1 + \sqrt{\left[\frac{k_1}{2} - 1\right]^2 - 1}\right\} \tag{2.9}$$

which is to the first order independent of frequency.

The Kukielka multivibrator uses a grounded capacitor topology and separates the threshold and current steering circuits to achieve a CCO with a TC of < 60 ppm/°C at frequencies up to 20 MHz and a linearity of < 3 %.

### 2.3.2 4046 Type Multivibrator

An example of a CMOS mulivibrator based on the grounded capacitor topology can be found in the VCO used for the 4046 PLL [14,20]. The RCA 4046's VCO [20] is capable of operating at frequencies up to 1.5 MHz over a control range of several decades with a linearity of about 1 % and has a TC of ≈ 200 ppm/°C.

Consider the simplified schematic of the 4046 type CCO [14] shown in Fig. 2.4. At initial power up the capacitor is discharged and the flipflop is in a random state determined by noise. Let $Q$ be *HIGH* ( $\bar{Q}$ is *LOW* ), this forces N1, P2 to be *ON* and N2, P1 to be *OFF* resulting

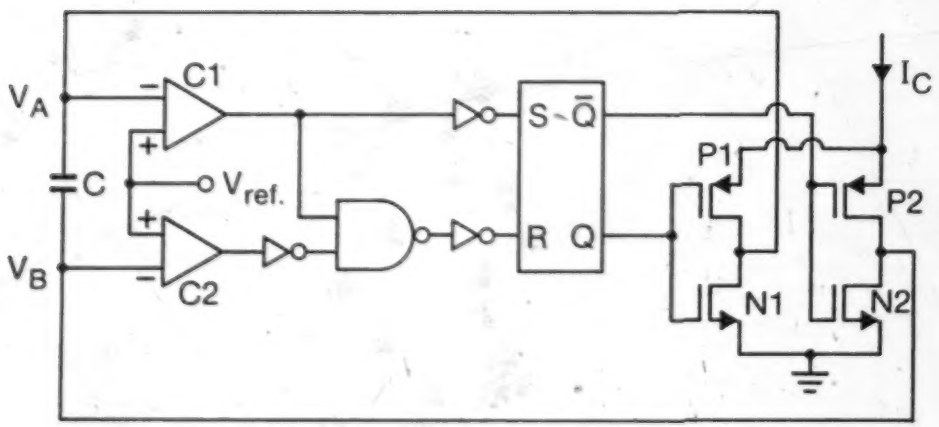


**Figure 2.4 4046 Type Multivibrator**

in $V_A$ being held at ground and $V_B$ to increase linearly with a slope of $I_C/C$. When $V_B$ reaches $V_{REF}$, the threshold of comparator C2, the output of the SR flipflop changes state and N1, P2 turn *OFF* and N2, P1 turn *ON*. Now $V_B$ is held fixed at the ground potential and $V_A$ swings to one diode drop below ground. The point $V_A$ attempts to swing to $V_{REF}$ below ground (since the voltage on the capacitor cannot change instantly) but is limited to one diode drop below ground by the parasitic PN junction formed by the drain diffusion/p-well of N1. From one diode drop below ground $V_A$ charges linearly with a slope of $I_C/C$ until it reaches the threshold ($V_{REF}$) of comparator C1 at which point the state of the flipflop changes and the process repeats. Every half cycle the capacitor is charged through a voltage of $V_{REF} + V_{BE,ON}$ by a current of $I_C$, therefore the frequency of oscillation is given by

$$f_o = \frac{I_C}{2\,C\,(\,V_{REF} + V_{BE,ON}\,)} \quad . \tag{2.10}$$

The reference voltage is chosen to be (see [14] for bias circuit)

$$V_{REF} = a\,V_{CC} - V_{BE,ON} \quad , \tag{2.11}$$

(where $a$ is a constant), as a result the frequency is independent of the base emitter drop (which has a large temperature coefficient) and becomes

$$f_o = \frac{I_C}{2\,C\,a\,V_{CC}} \quad . \tag{2.12}$$

The maximum frequency of operation of the 4046 type is ≈ 1.5 MHz. The primary frequency limitation is the switching delays of the threshold circuit formed by the comparators and the logic. As the switching delays approach the same order of magnitude as the period of oscillation the linearity of the control characteristic is degraded.

## 2.4 Conclusion

The emitter coupled multivibrator is based on a floating capacitor structure and provides a simple and compact circuit capable of high frequency operation with wide range and good linearity of frequency control. The CMOS Wakayama multivibrator also utilizes a floating capacitor structure and has been shown to be capable of very high frequency operation with good linearity and low jitter. Unfortunately, the circuitry is exceedingly complex and requires considerable chip area. Of the grounded capacitor topologies, the bipolar multivibrator developed by Kukielka has shown good performance in terms of linearity, range of frequency control, high frequency capability and has a low temperature coefficient even at high frequencies. Performance of CMOS grounded capacitor multivibrators such as the 4046 type have typically been degraded by switching delays which has limited operation to below approximately 1.5 MHz.

From this review two interesting observations can be made: first no CMOS multivibrators based on the emitter coupled structure have appeared, and second, grounded capacitor multivibrators have the potential for good performance as witnessed by the Kukielka design but the CMOS counterparts have not achieved comparable performance. The

wide range of control, good linearity, high frequency capability, and simplicity of design of the emitter coupled multivibrator provides the incentive to investigate its CMOS equivalent (Chp. 3), the source coupled multivibrator. One problem with the CMOS grounded capacitor multivibrators is switching delays. The Kukielka multivibrator (bipolar) makes use of a very simple Schmitt trigger structure in order to minimize delays, whereas the 4046 type multivibrator (CMOS) has a relatively complex threshold circuit which increases switching delays. It is of interest therefore to investigate new CMOS grounded capacitor structures which have simpler and therefore faster threshold circuits. Such a circuit will be presented in Chapter 4.

## 3.0 Source Coupled Multivibrator

### 3.1 Introduction to the Source Coupled Multivibrator

As described in Chapter 2, a popular current controlled oscillator in bipolar technology is the emitter coupled multivibrator. Its popularity stems from its high frequency capability, good range and linearity of frequency control, and its simplicity of design. To the author's knowledge, no published analysis or use of the CMOS equivalent of the emitter coupled mulivibrator, the source coupled multivibrator (SCM), has appeared in the literature. It was desirable to investigate the source coupled multivibrator , shown in Fig. 3.1(a), because of its simplicity and potential for high frequency operation.

The emitter coupled multivibrator's high frequency capability is a result of its all-npn construction, non-saturated operation, and small signal swings [9,16]. Although the SCM cannot benefit from the non-saturated operation due to different modes of operation between the bipolar transistor and the MOSFET, benefits can be obtained from the low signal swings. In CMOS circuitry the primary speed limitation for switching is the time required to charge/discharge parasitic node capacitance [21]. Therefore, reduced signal swings will improve switching times. Even though the required operating frequency of an oscillator may not be very high, high frequency capability is desirable since the influence of switching delays is minimized. As the period of oscillation approaches the same order of magnitude as the switching delays, the linearity and range of the CCO is degraded.

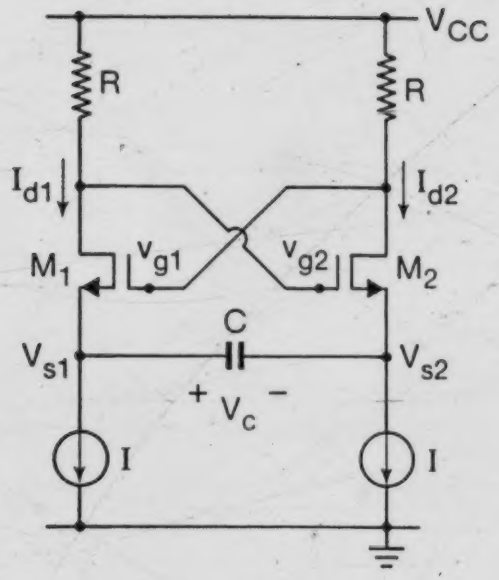


Figure 3.1(a)

Basic Source Coupled Multivibrator

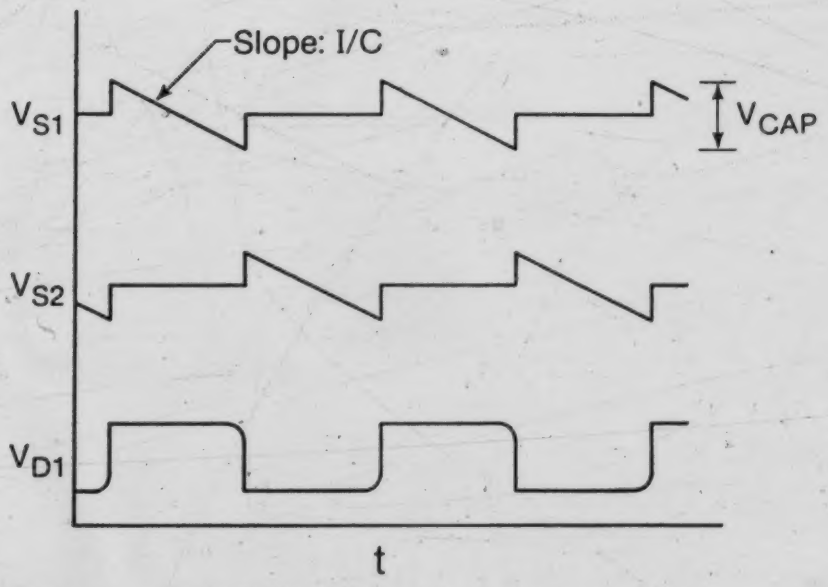


Figure 3.1(b) Typical Waveforms

This is best illustrated by considering the following equation for frequency:

$$f_o = \frac{1}{T} = \frac{1}{T_o + T_{SD}} \qquad (3.1)$$

where

$$T_o = \frac{2\,C\,V_{HYST}}{I} \qquad (3.2)$$

and

$T_{SD}$ = total switching delay.

At low frequencies ($T_o \gg T_{SD}$) the frequency is inversely proportional to $T_o$ and can be controlled linearly with $I$. At high frequencies ($T \ll T_{SD}$) the frequency of oscillation is constant at $1/T_{SD}$ and $I$ has no control over frequency. In the region between these two extremes the frequency of oscillation is related in a nonlinear manner to $I$. Therefore, for a CCO to have linear control of frequency with current the switching delays must be kept much shorter then the period of oscillation ($T_o$). Minimization of switching delays is also important for thermal stability since the delays are a function of transistor parameters, and parasitic node resistances and capacitances all of which are temperature dependent.

The core of the basic SCM (Fig. 3.1(a)) is formed by a total of two transistors, two loads, two current sources, and one capacitor.

This provides a very simple and compact circuit, which helps minimize the circuit's switching delays.

The analysis of the source coupled multivibrator will be divided into two parts. First, an approximate analysis of the circuit will be carried out for the specific case where all transistors have their sources tied to the substrate. This analysis will provide insight into the basic performance of the SCM without the complication of the body effect. Finally a full and detailed analysis of the SCM will be carried out with the body effect included. The body effect only appears on the primary devices M1 and M2.

The shape of the control characteristic of frequency with current depends on the type of load presented to the drains of M1 and M2. Three type of load configurations will be examined:

(1) purely resistive load

(2) combined active/resistive load

(3) purely active load.

These are shown in Fig. 3.2(a), (b), and (c) respectively.

## 3.2 Basic Operation

The basic operation of the source coupled multivibrator will now be briefly explained. The basic circuit is shown in Fig. 3.1(a) and some typical waveforms are shown in Fig. 3.1(b).

The circuit is quasistable. The output, taken from the drain node of M1 (drain of M2 provides the complementary output), spends most of each half cycle in one quasistable state and switches rapidly at the end of every half cycle to the other state. The frequency of

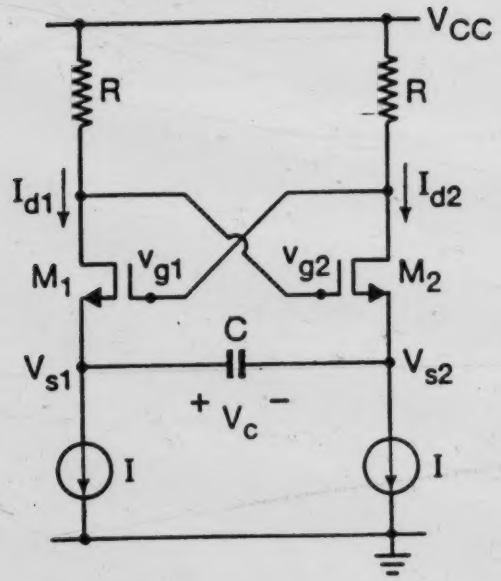


Figure 3.2 Load Configurations

(a) Resistive Load

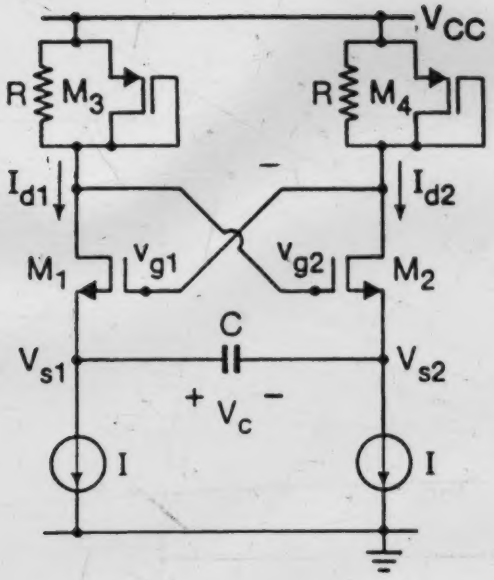


or

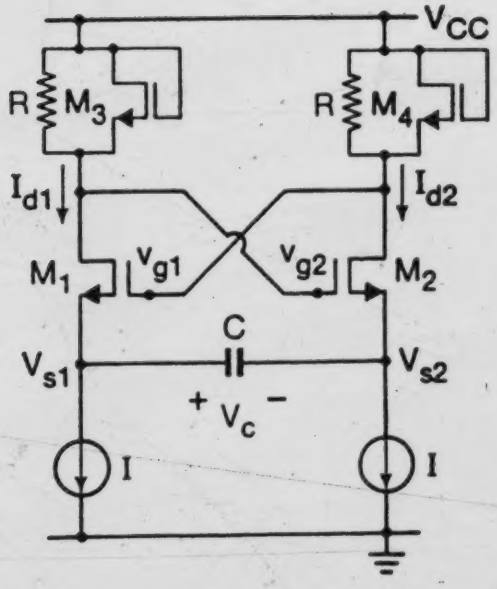


**Figure 3.2 Load Configurations**

(b) Active/Resistive Load

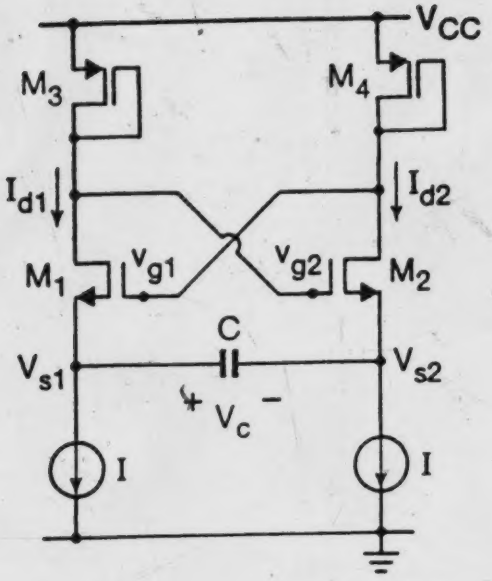


or

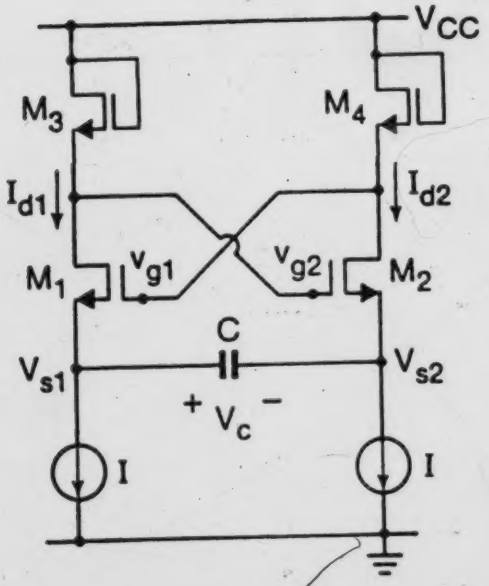


**Figure 3.2 Load Configurations**

(c) Active Load

oscillation is found by determining when the circuit switches from one quasistable state to the other. Overall the circuit operation is highly nonlinear, but during a very short period before each transition the circuit enters a region of linear operation. This region of linearity is exploited to allow the frequency of oscillation to be determined.

Consider the transition of M1 from *ON* to *OFF* and M2 from *OFF* to *ON*. Unless specified otherwise all the analysis will be done for this transition, the opposite transition is a mirror image due to the circuit's symmetry and will not be considered further. Initially M1 is *ON* and passes the current of $2I$ and M2 is off and passes no current. As a result the capacitor is charged by a current of $I$. With M2 *OFF*, the source voltage of M1 is fixed at one gate-source voltage drop below $V_{CC}$. The voltage at the source of M2 is free to change and decreases linearly with a slope of $I/C$. Eventually the source voltage of M2 has dropped such that the gate-source voltage of M2 is equal to the threshold voltage (the gate of M2 is held fixed by the voltage drop across the drain load of M1). Now M2 begins to conduct and its drain voltage drops, this decreases the gate-source voltage of M1 which causes the gate voltage of M2 to increase. This in turn increases the current through M2 and so on. At a critical level of current through M2, the loop gain of the feedback loop exceeds +1 and the circuit undergoes regenerative switching. Now the source voltage of M2 is held fixed and since the voltage across the capacitor cannot change instantaneously the source of M1 is forced to $V_{CAP}$ above the source of M2. $V_{CAP}$ is the voltage across the capacitor

at the instant of regenerative switching. Now the circuit is in another quasistable state with M1 *OFF* and M2 *ON*. The mirror image of the previous cycle now occurs and the circuit enters astable operation.

The general expression for the frequency of oscillation for the SCM is given by

$$f_o = \frac{I}{4\ C\ V_{CAP}} \qquad (3.3)$$

where $V_{CAP}$ is the voltage across the capacitor at the point of regenerative switching.

### 3.3 Analysis of SCM With No Body Effect

The source coupled multivibrator will now be analyzed for the case where all transistors have their sources tied to the substrate in order to eliminate the body effect. All three load configurations will be included in the analysis.

For the following analysis the transition under consideration will be the one where M1 turns from *ON* to *OFF* and M2 turns from *OFF* to *ON*. One simplifying assumption made for this analysis is that regenerative switching occurs instantly when the gate-source voltage of M2 reaches the threshold voltage. This analysis is intended to provide only a rough approximation of the circuit's performance in order to aid intuitive understanding of its behaviour. It should not be used as a means of calculating the operating frequency with any degree of accuracy.

The general approach taken in the analysis is to first determine the source voltages of M1 and M2 at the instant of transition. These are then used to calculate the voltage across the capacitor, from which the frequency of oscillation is determined.

### 3.3.1 Purely Resistive Load

The first configuration to be studied will be the case where the drain loads of M1 and M2 are purely resistive (shown in Fig. 3.2(a)). Let the resistors be of value *R*.

Just before switching occurs M1 is *ON* and M2 is *OFF*, as a result

$$I_{d1} = 2I \tag{3.4}$$

$$I_{d2} = 0 \ . \tag{3.5}$$

The source voltage of M1 is found to be

$$V_{s1} = V_{CC} - V_{tno} - \sqrt{\frac{2I}{\beta_n}} \ . \tag{3.6}$$

This is obtained from the current characteristic of the MOSFET which is defined as [9]:

$$I_d = \beta_n (V_{GS} - V_{tno})^2 \tag{3.7}$$

where

$$\beta_n = \frac{\mu C_{ox}}{2} \frac{W}{L} \tag{3.8}$$

and $V_{tno}$ is the threshold voltage of the NMOS FET (with $V_{SB}$=0). The term $\beta_n$ can be considered to be the gain coefficient of the MOSFET. At the instant of regenerative switching

$$V_{gs2} = V_{tno} \quad , \tag{3.9}$$

therefore the source voltage of M2 is:

$$V_{s2} = V_{CC} - 2IR - V_{tno} \quad . \tag{3.10}$$

At the instant of regenerative switching the voltage across the capacitor is

$$V_{CAP} = V_{s1} - V_{s2} \tag{3.11}$$

and so,

$$V_{CAP} = 2IR - \sqrt{\frac{2I}{\beta_n}} \quad . \tag{3.12}$$

From which the frequency of oscillation can be found to be:

$$f_o \approx \frac{I}{4\,C\,V_{CAP}} = \frac{I}{4\,C\left[2IR - \sqrt{\frac{2I}{\beta_n}}\right]} \tag{3.13}$$

and, if

$$R \gg \sqrt{\frac{1}{2I\beta_n}} \quad , \tag{3.14}$$

then

$$f_o \approx \frac{1}{8\,R\,C} \quad . \tag{3.15}$$

Therefore the SCM with a purely resistive load can be operated as a fixed frequency oscillator, the frequency of which is dependent only on $R$ and $C$.

### 3.3.2 Combined Resistive/Active Load

Let the load be the parallel combination of a resistor and an NMOS or PMOS transistor connected as shown in Fig. 3.2(b). Consider the case where the transistor is PMOS. The derivation for the case of an NMOS transistor is exactly the same except for nomenclature.

Since no current is passed by M2 before the transition, the active device M4 is *OFF*. Therefore at the instant of transition the source voltage for M1 is the same as that for the purely resistive load case. The expression is repeated here for convenience

$$V_{s1} = V_{CC} - V_{tno} - \sqrt{\frac{2I}{\beta_n}} \quad . \tag{3.16}$$

Transistor M1 passes a current of $2I$ just before the transition and hence the active device M3 is *ON* (assuming $2IR > V_{tpo}$). If the assumption that

$$R \gg \frac{1}{g_{m3}} \quad , \tag{3.17}$$

is made, where $g_{m3}$ is the transconductance of M3, then the current through M3 can be taken as $\approx 2I$. The source voltage of M2 can then be written as

$$V_{s2} = V_{CC} - |V_{tpo}| - \sqrt{\frac{2I}{\beta_p}} - V_{tno} \quad . \tag{3.18}$$

Therefore, the voltage across the capacitor is

$$V_{CAP} = |V_{tpo}| + \sqrt{2I} \left[ \frac{1}{\sqrt{\beta_p}} - \frac{1}{\sqrt{\beta_n}} \right] \quad , \tag{3.19}$$

and the frequency of oscillation is

$$f_o \cong \frac{I}{4\,C\left[\,|V_{tpo}| + \sqrt{2I}\left(\frac{1}{\sqrt{\beta_p}} - \frac{1}{\sqrt{\beta_n}}\right)\right]} \quad . \tag{3.20}$$

If

$$|V_{tpo}| \gg \sqrt{2I}\left(\frac{1}{\sqrt{\beta_p}} - \frac{1}{\sqrt{\beta_n}}\right) , \tag{3.21}$$

(which is true if $\beta_n = \beta_p$) then:

$$f_o \approx \frac{I}{4\,C\,|V_{tpo}|} \quad . \tag{3.22}$$

Therefore the SCM with a combined active/resistive load has the potential to operate with linear control of frequency by current $I$.

### 3.3.3 Purely Active Load

The final load configuration considered is that of an NMOS or PMOS transitor alone, connected as shown in Fig. 3.2(c). The case of a PMOS load will be considered.

Because of leakage currents through the nominally *OFF* transistor M2 the voltage at the gate of M1 is one threshold drop below $V_{CC}$. As a result the source voltage of M1 is fixed at

$$V_{s1} = V_{CC} - |V_{tpo}| - V_{tno} - \sqrt{\frac{2I}{\beta_n}} \quad , \tag{3.23}$$

and the source voltage of M2 is

$$V_{s2} = V_{CC} - |V_{tpo}| - \sqrt{\frac{2I}{\beta_p}} - V_{tno} \quad . \tag{3.24}$$

From (3.23) and (3.24) the voltage across the capacitor is found to be

$$V_{CAP} = \sqrt{2I}\left[\frac{1}{\sqrt{\beta_p}} - \frac{1}{\sqrt{\beta_n}}\right] \tag{3.25}$$

and so the frequency of oscillation is

$$f_o = \frac{\sqrt{I}}{4\sqrt{2}\,C\left[\frac{1}{\sqrt{\beta_p}} - \frac{1}{\sqrt{\beta_n}}\right]} \quad . \tag{3.26}$$

Note that if $\beta_n = \beta_p$ then $f_o \to \infty$. The SCM with a purely active load produces a CCO with a control characteristic where the frequency has a square root dependence on the control current.

### 3.3.4 Discussion of Results

Due to the simplifying assumptions made, these results can, at best, be considered to be approximations to the circuits' true behaviour. However, they do provide useful insight into the SCM's performance. With proper choice of parameters: the purely resistive load SCM can be used as a fixed frequency oscillator; the combined active/resistive load SCM can be operated as a CCO with linear control of frequency with current; and the purely active load SCM provides a CCO that has a square root dependence of frequency on current. In all cases, improper choice of parameters will lead to a CCO with nonlinear

variation of frequency with the control current.

### 3.4 Analysis of SCM Including Body Effect

Due to technological and design constraints, it is not always possible to eliminate the body effect (i.e., the variation of the threshold voltage with the source-substrate bias) on all transistors in a circuit. In order to eliminate body effect for a transistor it is necessary to tie the source and substrate together. This is available only for devices of one polarity in standard CMOS processes ( i.e. NMOS in a p-well technology) and requires these devices to be placed in separate wells in the substrate. As a result more chip area is consumed, and device matching will be reduced. It is therefore desireable to obtain analytical expressions for the frequency of the SCM that include the body effect.

For this analysis the assumption made previously (Sect. 3.3), that regenerative switching occurs at the moment when $V_{gs,M2} = V_{tn}$, will no longer be used. The threshold points for regenerative switching will be determined from the condition that at the switching point the loop gain of the feedback loop becomes equal to +1 [11,16,22].

#### 3.4.1 Determination of Loop Gain

The condition for transition from one quasistable state to another is

$$A_{LOOP} = 1 \tag{3.27}$$

where the loop gain is defined as

$$A_{LOOP} = \frac{v_{d1}''}{v_{d1}'} \quad . \tag{3.28}$$

The loop gain is found by breaking the feedback loop at the drain of M1, introducing a voltage source $v_{d1}'$ on the gate of M2, and determining the resulting voltage $v_{d1}''$ at the drain of M1.

From the point where M2 is just *OFF* (i.e., $V_{gs2} = V_{tn}$) to the point where the current through M2 has reached the level required for regenerative switching, the circuit is in linear operation. The small signal equivalent circuit for this region is shown in Fig. 3.3. For now the loads at the drains of M1 and M2 will be considered to be arbitrary devices with impedances of $Z_1$ and $Z_2$. The specific load cases will be dealt with later.

The following assumptions are made in deriving the small signal equivalent circuit:

(1) the capacitor $C$ appears as a short circuit during the short time of the transient since the charging time is considered to be greater then the switching time,

(2) the body transconductance of M1 and M2 are not included since the sources remain at approximately the same level during the time just before the transient,

(3) the total equivalent output impedance of the current sources is given by $r_o$ and is high,

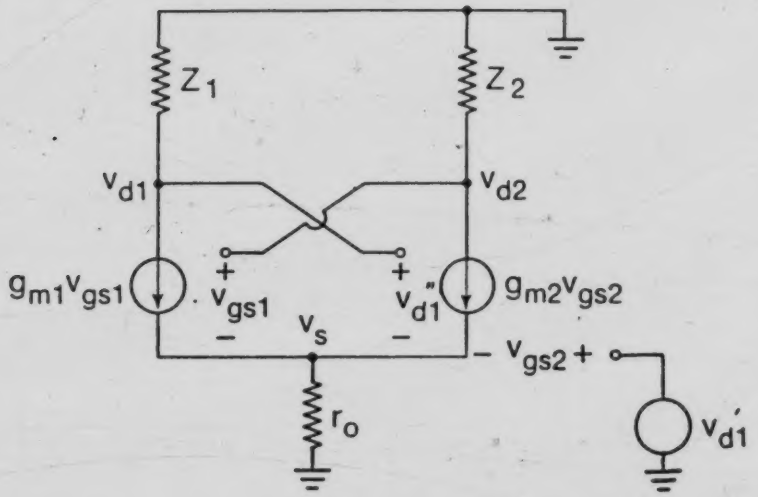


Figure 3.3 Small Signal Equivalent Circuit for Loop Gain Calculation

(4) the drain loads of M1 and M2 have an impedance of $Z_1$ and $Z_2$ respectively.

(5) The charging current for the capacitor is constant for each half cycle, i.e. the current diverted (into M2) before regenerative switching occurs is negligible.

Let:

$$v_{gs1} = v_{g1} - v_s = v_{d2} - v_s \tag{3.29}$$

$$v_{gs2} = v_{g2} - v_s = v_{d1}' - v_s \tag{3.30}$$

where:

$$v_s = \left[ g_{m1} v_{gs1} + g_{m2} v_{gs2} \right] r_o \quad . \tag{3.31}$$

Substituting (3.31) into (3.30) yields:

$$v_{gs2} = \frac{v_{d1}' - g_{m1} r_o v_{gs1}}{1 + g_{m2} r_o} \quad . \tag{3.32}$$

Similarly,

$$v_{gs1} = \frac{v_{d2} - g_{m2} r_o v_{gs2}}{1 + g_{m1} r_o} \tag{3.33}$$

where:

$$v_{d2} = - g_{m1} R_1 v_{gs2} \quad . \tag{3.34}$$

Combining (3.32), (3.33), and (3.34) yields:

$$v_{gs1} = \frac{-g_{m2}(Z_2+r_o)v_{d1}'}{(1+g_{m1}r_o)(1+g_{m2}r_o) - g_{m1}g_{m2}(Z_2+r_o)r_o} \tag{3.35}$$

and, using

$$v_{d1}'' = -g_{m1} Z_1 v_{gs1} \quad , \tag{3.36}$$

the loop gain is found to be:

$$A_{LOOP} = \frac{g_{m1}g_{m2}Z_1(Z_2+r_o)}{(1+g_{m1}r_o)(1+g_{m2}r_o)-g_{m1}g_{m2}(Z_2+r_o)r_o} \quad . \tag{3.37}$$

Rewriting the loop gain as

$$A_{LOOP} = \frac{g_{m1}g_{m2}Z_1}{\frac{1}{(Z_2+r_o)} + (g_{m1}+g_{m2})\frac{r_o}{(Z_2+r_o)} - \frac{g_{m1}g_{m2}r_oZ_2}{(Z_2+r_o)}} \tag{3.38}$$

and using the assumption that $r_o \blacktriangleright \infty$, the loop gain simplifies to

$$A_{LOOP} = \frac{g_{m1}g_{m2}Z_1}{(g_{m1}+g_{m2}) - g_{m1}g_{m2}Z_2} \tag{3.39}$$

At the onset of regenerative switching $A_{LOOP} = 1$, therefore, the condition of switching is given as

$$\frac{1}{g_{m1}} + \frac{1}{g_{m2}} = Z_1 + Z_2 \tag{3.40}$$

This expression is valid for all loads.

### 3.4.2 Determination of Oscillation Frequency

The basic steps used in calculating the frequency are:

(1) determine the currents through M1 and M2 at the point of regenerative switching using the condition that loop gain is 1 (3.40),

(2) use these currents to find the source voltages of M1 and M2 at the transition point,

(3) from the source voltages determine the voltage across the capacitor and find the frequency of oscillation.

An attempt will be made to keep the derivations of the equations as general as possible. First a general expression will be presented and then the specific load configurations will be examined.

The current levels in M1 and M2 at the instant of transition will now be calculated using (3.40) as the condition of transition. Let

$$Z_1 + Z_2 = R_{eq} \qquad (3.41)$$

and

$$g_{m1} = 2\sqrt{\beta_n I_{d1}} \qquad (3.42)$$

$$g_{m2} = 2\sqrt{\beta_n I_{d2}} \qquad (3.43)$$

The condition for regenerative switching now becomes

$$\sqrt{I_{d1}} + \sqrt{I_{d2}} = 2 R_{eq} \sqrt{\beta_n} \sqrt{I_{d1} I_{d2}} \qquad (3.44)$$

From the circuit topology, an additional constraint:

$$I_{d1} + I_{d2} = 2 I \qquad (3.45)$$

is obtained. Combining (3.44) and (3.45), the currents of M1 and M2 can be obtained:

$$I_{d1} = I \left( 1 + \sqrt{1 - 4 m_{th}^2} \right) \qquad (3.46)$$

$$I_{d2} = I \left( 1 - \sqrt{1 - 4 m_{th}^2} \right) \qquad (3.47)$$

where:

$$m_{th} = \frac{1}{\sqrt{1 + 8\, R_{eq}^2\, \beta_n\, I} - 1} \quad . \tag{3.48}$$

If $m_{th}$ is small (typically) then the expressions for $I_{d1}$ and $I_{d2}$ can be simplified to:

$$I_{d1} \cong 2\, I\, (1 - m_{th}^2) \tag{3.49}$$

$$I_{d2} \cong 2\, I\, m_{th}^2 \quad . \tag{3.50}$$

The expression for $m_{th}$ will now be determined for the three different load configurations.

(1) Purely Resistive Load

The load is purely resistive and $Z_1 = Z_2 = R$. Therefore

$$R_{eq} = 2\, R \tag{3.51}$$

and from (3.48)

$$m_{th} = \frac{1}{\sqrt{1 + 32\, R^2\, \beta_n\, I} - 1} \quad . \tag{3.52}$$

(2) Combined Active/Resistive Load

Consider that the load is formed by a resistor in parallel with a PMOS transistor, connected as shown in Fig. 3.2(b). When M1 is *ON* and M2 is *OFF* the small signal load impedances become:

$$Z_1 = \frac{R \,/\, g_{m3}}{R + \dfrac{1}{g_{m3}}} \tag{3.53}$$

$$Z_2 = R \tag{3.54}$$

where $g_{m3}$ is the transconductance of the load device M3. It is given by:

$$g_{m3} \cong 2\,\beta_p \sqrt{V_{cc} - V_{G2} - |\,V_{tpo}\,|} \tag{3.55}$$

where:

$$V_{G2} \cong V_{CC} - |\,V_{tpo}\,| - \frac{\sqrt{1 + 4\,\beta_p\,R\,(\,2\,I\,R - |\,V_{tpo}\,|\,)} - 1}{2\,\beta_p\,R} \tag{3.56}$$

These expressions were derived using the assumption that $I_{d1} \cong 2\,I$, which is valid if $m_{th}$ is small. The total equivalent impedance of the drain loads becomes (3.53 and 3.54 into 3.41):

$$R_{eq} = R\left[\frac{R\,(\,2 + g_{m3}\,R\,)}{1 + g_{m3}\,R}\right]. \tag{3.57}$$

Using (3.57) in (3.48) yields:

$$m_{th} = \frac{1}{\sqrt{1 + 8\left[R\left[\frac{R\,(\,2 + g_{m3}\,R\,)}{1 + g_{m3}\,R}\right]\right]^2 \beta_n\,I} - 1} \tag{3.58}$$

(3) Purely Active Load

For the purely active load a better understanding of the condition for switching can be obtained by looking at the basic expression for $A_{LOOP} = 1$. The equivalent small signal impedances of the load devices M3 and M4 are

$$Z_1 = \frac{1}{g_{m3}} \tag{3.59}$$

$$Z_2 = \frac{1}{g_{m4}} \tag{3.60}$$

The condition for switching, (3.40), now becomes

$$\frac{1}{g_{m1}} + \frac{1}{g_{m2}} = \frac{1}{g_{m3}} + \frac{1}{g_{m4}} \tag{3.61}$$

which can be rewritten as

$$\frac{1}{\sqrt{\beta_n}}\left[\frac{1}{\sqrt{I_{d1}}} + \frac{1}{\sqrt{I_{d2}}}\right] = \frac{1}{\sqrt{\beta_p}}\left[\frac{1}{\sqrt{I_{d1}}} + \frac{1}{\sqrt{I_{d2}}}\right] . \tag{3.62}$$

This expression will be valid if one of the following conditions are true:

(1) $\beta_n = \beta_p$

(2) $\beta_n$ and $\beta_p \rightarrow 0$

(3) $I_{d1}$ or $I_{d2} \rightarrow 0$.

From the approximate analysis carried out in Section 3.3.3 it is seen that $f_o \rightarrow \infty$ if $\beta_n = \beta_p$. Physically the $\beta$'s cannot be equal to zero. Therefore, the only valid solution is when $I_{d2} = 0$ (in the mirrored transition $I_{d1} = 0$). This implies that once $V_{GS2} = V_{tn}$ the circuit instantly switches. Therefore

$$m_{th} = 0 \tag{3.63}$$

for the case of purely active loads.

Once $m_{th}$ has been found, all that is required to determine the frequency of oscillation, is the voltages at sources of M1 and M2.

The general expression for the source voltage of either M1 or M2 is

$$V_{Si} = \frac{2\,V_{ni} + \gamma^2 - \gamma\sqrt{\gamma^2 + 4\,V_{ni} + 8\,|\phi_f|}}{2} \qquad (i = 1,2) \qquad (3.64)$$

where

$$V_{ni} = V_{Gi} + \gamma\sqrt{2\,|\phi_f|} - V_{tno} - \sqrt{\frac{I_{di}}{\beta_n}} \qquad (i = 1,2) \qquad (3.65)$$

The term $V_{Gi}$ is the gate voltage of M1 or M2 and must be determined from the load configuration under consideration. The above expressions follow from the general current expressions of the MOSFET [34] and will be repeated here for convenience

$$I_{di} = \beta_n \left[ V_{Gi} - V_{Si} - V_{tni} \right]^2 \qquad (3.66)$$

$$V_{tni} = V_{tno} + \gamma \left[ \sqrt{2\,|\phi_f| + V_{SBi}} - \sqrt{2\,|\phi_f|} \right] . \qquad (3.67)$$

The gate voltage, $V_{Gi}$, will now be determined for the three load configurations:

(1) Purely Resistive Load

For the resistive load the expressions for the gate voltages of M1 and M2 are simply:

$$V_{G1} = V_{CC} - I_{d2}\,R \qquad (3.68)$$

$$V_{G2} = V_{CC} - I_{d1}\,R \; . \qquad (3.69)$$

(2) Combined Active/Resistive Load

Before the transition the load device M4 is *OFF* (i.e.

$V_{gs4} < I_{d2}R < V_{tpo}$) and the gate voltage of M1 is given by:

$$V_{G1} = V_{CC} - I_{d2} R \quad . \tag{3.70}$$

The gate voltage of M2 was derived earlier (3.56) and is simply repeated here:

$$V_{G2} \cong V_{CC} - |V_{tpo}| - \frac{\sqrt{1 + 4 \beta_p R ( I_{d1} R - |V_{tpo}| )} - 1}{2 \beta_p R} \tag{3.71}$$

(3) Purely Active Load

Since $m_{th}$ is zero for the case of the purely active load, the gate voltages are simply

$$V_{G1} = V_{CC} - |V_{tpo}| \tag{3.72}$$

and

$$V_{G2} = V_{CC} - |V_{tpo}| - \sqrt{\frac{2I}{\beta_p}} \quad . \tag{3.73}$$

Once the gate voltages of M1 and M2 have been found using the appropriate expressions the source voltages can be found using (3.64), and finally the frequency of oscillation can be calculated using

$$f_o = \frac{I}{4 C V_{CAP}} \tag{3.74}$$

where

$$V_{CAP} = V_{S1} - V_{S2} \quad . \tag{3.75}$$

## 3.5 Experimental Verification

Verification of the results of Section 3.4 was carried out by investigating experimentally two load configurations: purely resistive, and the combined active/resistive load. The experimental circuits are shown in Fig. 3.4 and 3.5 respectively. The body effect was included in these circuits.

Although this work is intended for SCMs realized in integrated form this was not possible due to time constraints. Instead the circuits were constructed using matched pairs of NMOS and PMOS FETs available from Ferranti/Interdesign as the MO415 [14]. The substrate of each transistor pair is common (i.e. common p-well for the NMOS and common n-substrate for the PMOS) therefore the body effect for all the devices could not be removed.

The two experimental circuits are identical except for the load configuration. A PMOS load is used for the combined active/resistive load case to obtain better matching of the device $\beta$'s, as was required (3.19), in order to achieve a CCO with linear control of frequency with current. Every MO415 has a pair of NMOS and PMOS FETs; the $W/L$ ratios of the N and P-devices are chosen such that, nominally, $\beta_n \cong \beta_p$. To obtain the highest frequency of oscillation it would be desirable to use NMOS devices for the loads since $\mu_n > \mu_p$, but for the experimental work PMOS devices were chosen for the loads since better matching of $\beta$ was obtained between the N and P-devices of one chip

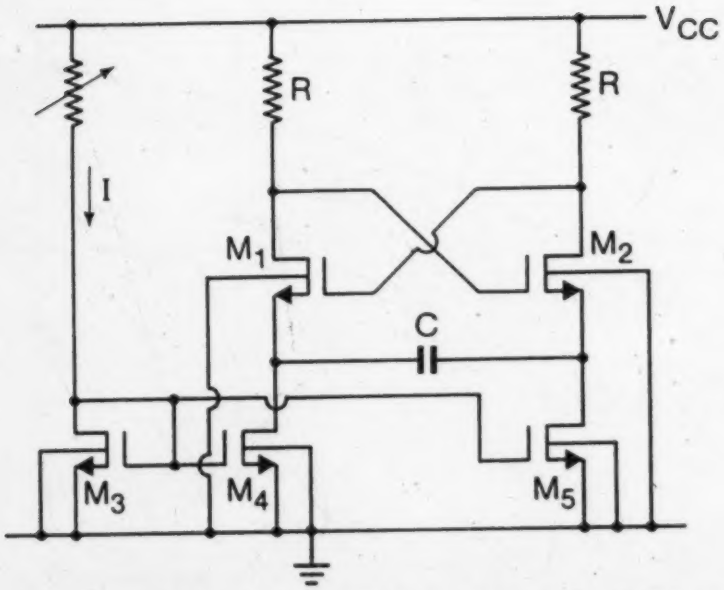


**Figure 3.4 Experimental Circuit with Purely Resistive Load**

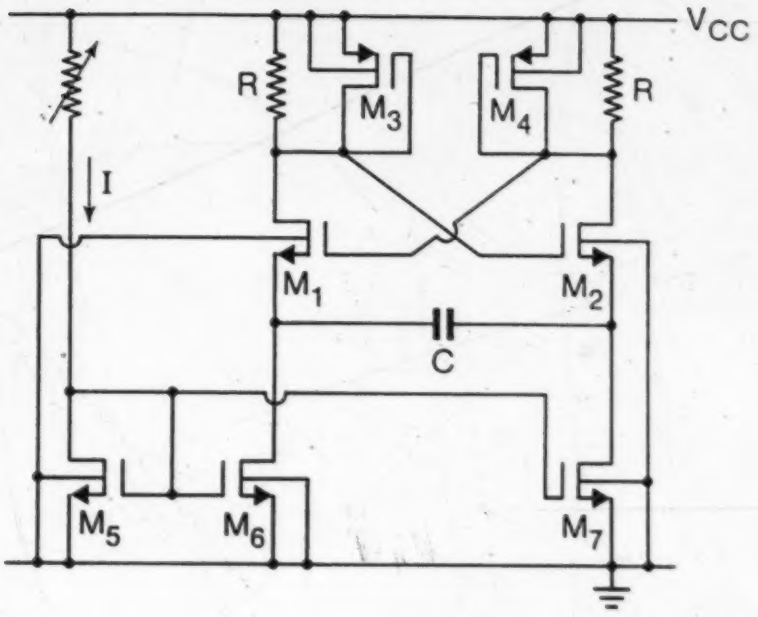


Figure 3.5 Experimental Circuit with Combined Active/Resistive Load

then between the N devices of two chips. The tradeoff of speed is made for linearity. The measured device parameters for M1, M2 (NMOS) and M3, M4 (PMOS) are found in Table 3.1. The other circuit parameters are found in Table 3.2.

### 3.5.1 Experiment 3.1: Purely Resistive Load

The source coupled multivibrator with a purely resistive load (Fig. 3.4) represents the simplest case and will be studied first. The frequency, $f_o$, versus current, $I$, for the range of $I$ from 50 to 300 $\mu$A was measured and the results are plotted in Fig. 3.6, along with the values of frequency predicted using (3.74).

A good match between the experimental results and theory was obtained over the region where the theoretical equations are valid. As the current $I$ increased above $\approx$ 150 $\mu$A M1 and M2 drop out of pinch off operation (for pinchoff operation $V_{DS} \geq V_{GS} - V_t$) and the theory is no longer valid. At low currents, i.e. $I < 50$ $\mu$A, the threshold coefficient $m_{th} \rightarrow 1/2$ causing $I_{d2} \rightarrow I$, the difference between the source voltages of M1 and M2 at the switching point goes to zero and $f_o \rightarrow \infty$, which was confirmed experimentally. The critical current, $I_{crit}$, where $f_o \rightarrow \infty$ can be found by equating $m_{th}$ to 1/2 in (3.58), and is given by:

$$I_{crit} = \frac{1}{4 R^2 \beta_n} \quad . \tag{3.76}$$

For the parameters given, $I_{crit} \approx 7.2$ $\mu$A. This corresponds well with the experimental results.

Over the region where the theory was valid ( $I \approx 15 \rightarrow 150$ $\mu$A )

| | NMOS | PMOS |
|---|---|---|
| W/L | 310/24 | 580/24 |
| $\beta^{*}$ ($\mu A/V^2$) | 110 | 110 |
| $\beta^{**}$ ($\mu A/V^2$) | 125 | 90 |
| $V_t$ (V) | 1.25 | 0.9 |
| $\gamma$ ($V^{1/2}$) | 1.8 | - |
| $\phi_f$ (V) | 0.3 | 0.3 |

* Measured at $|I_D| \approx 50$ $\mu$A and $|V_{SB}| \approx 0$

** Average over $|I_D| \approx 50 \rightarrow 1600$ $\mu$A and
$|V_{SB}| \approx 6$ V for NMOS
$|V_{SB}| \approx 0$ V for PMOS

\- see [25] for method of determining device parameters

TABLE 3.1 TRANSISTOR PARAMETERS FOR M1/M2 (NMOS) AND M3/M4 (PMOS) FOR EXP. 3.1 AND 3.2

| | EXP # 3.1 | EXP # 3.2 |
|---|---|---|
| R (k$\Omega$) | 18 | 18 |
| C (nF) | 8.7 | 8.2 |
| $V_{CC}$ (V) | 15 | 15 |

TABLE 3.2 CIRCUIT PARAMETERS FOR EXP. 3.1, AND 3.2

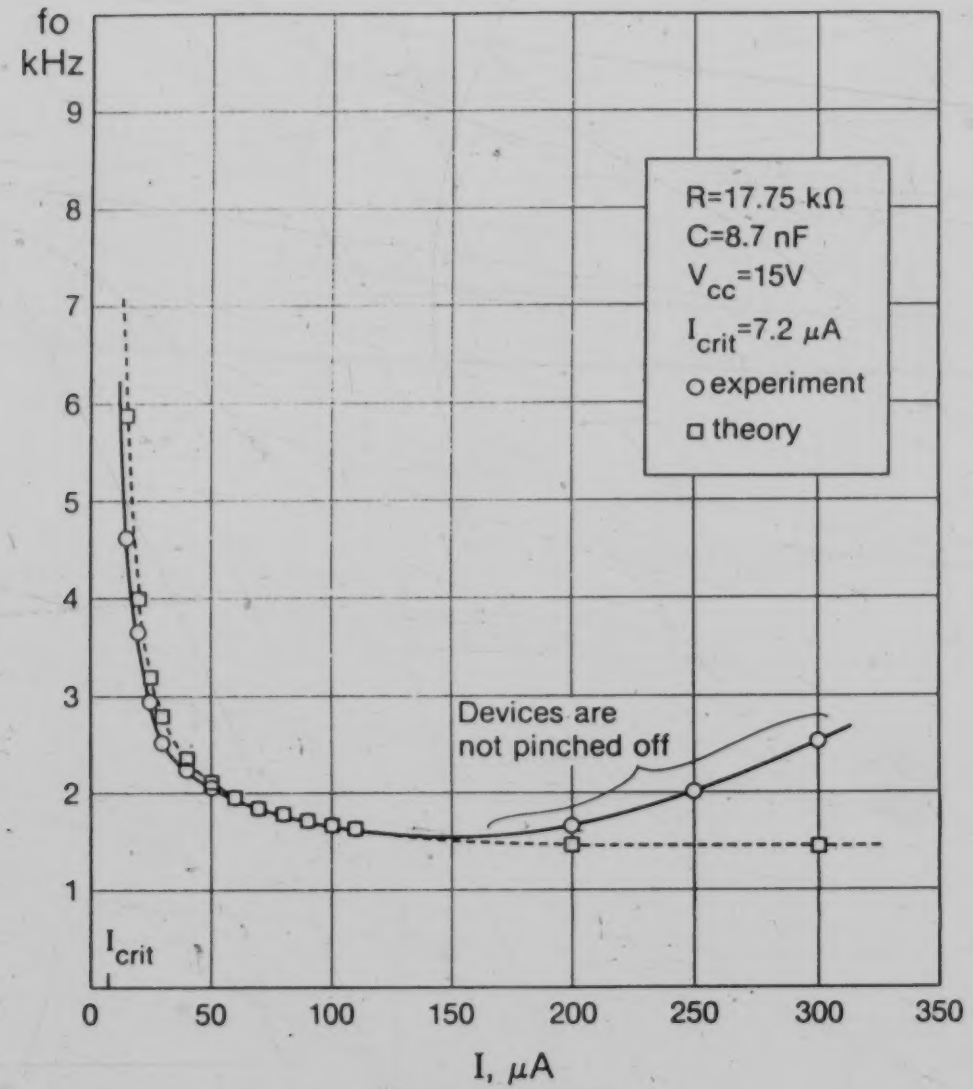


Figure 3.6 Frequency Characteristic for the Purely Resistive Load Case

good correlation between theory and experiment was obtained. The beginning of fixed frequency operation was seen just before the circuit dropped out of pinchoff operation.

### 3.5.2 Experiment 3.2: Combined Active/Resistive Load

The circuit for the combined active/resistive load configuration is shown in Fig. 3.5 and is identical to that used in Experiment 3.1 except that a PMOS load was connected in parallel with the resistor. All other circuit parameters remained the same. Every attempt was made to match the $\beta$'s of the NMOS and PMOS devices (i.e., $\beta_n = \beta_p$) so that the oscillator would have a linear frequency versus current characteristic.

The frequency was measured over a current range from $I = 50$ $\mu$A to 1600 $\mu$A and the results are plotted in Fig. 3.7 along with the theoretically predicted values of frequency calculated using the parameters given in Tables 3.1, and 3.2, and with $\beta_n = \beta_p = 110$ $\mu A/V^2$. These values for the $\beta$'s were measured experimentally at $I_D \approx 50$ $\mu$A and at $V_{SB} = 0$. Except at very low levels of current the theoretical calculations grossly overestimate the frequency; not even the shape of the frequency characteristic is predicted correctly. The theory predicts an approximately linear characteristic whereas the experimental results are decidedly nonlinear. Why is there such a large discrepancy? The theory proved to be quite accurate for the case of a purely resistive load, but now is totally in error.

An understanding of the origin of the discrepancy between theory and experiment can be obtained by considering (3.19), which is

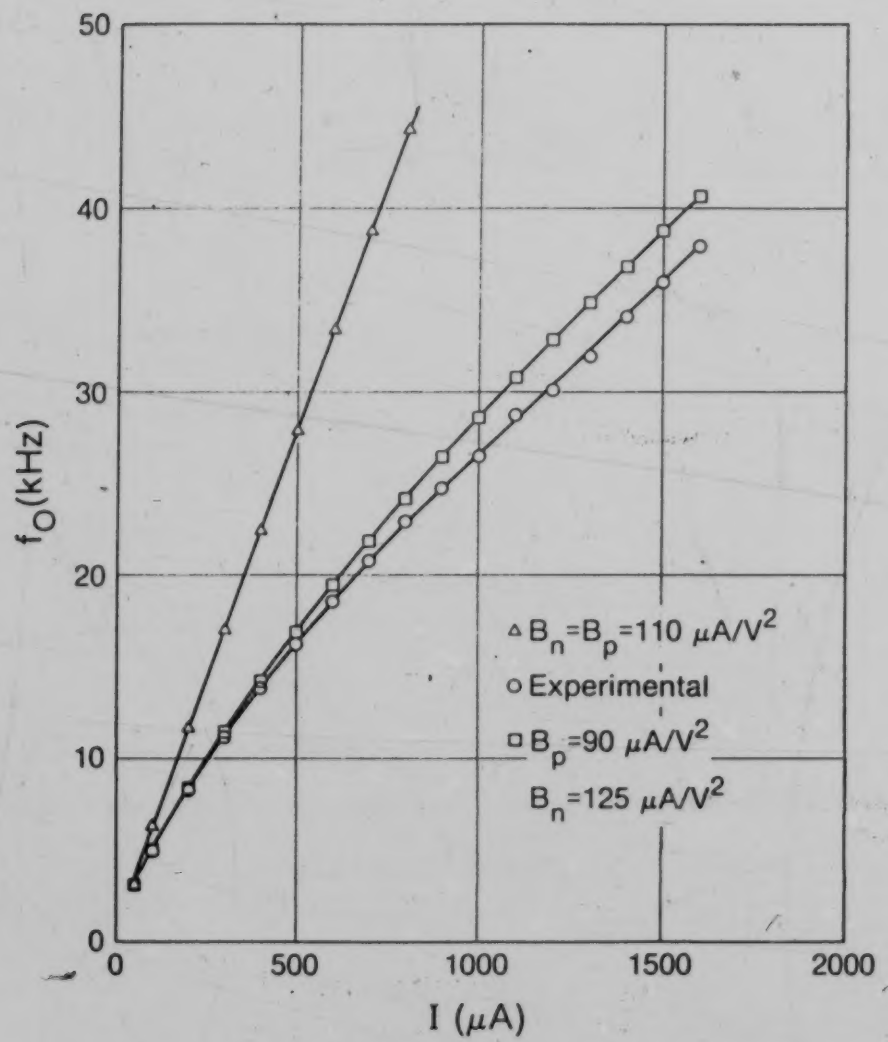


**Figure 3.7 Frequency Characteristic for the Combined Active/Resistive Load Case**

repeated here for convenience

$$V_{CAP} = |V_{tpo}| + \sqrt{2I}\left[\frac{1}{\sqrt{\beta_p}} - \frac{1}{\sqrt{\beta_n}}\right] . \qquad (3.77)$$

Even though this expression was derived for devices with no body effect, the trends it suggests are still valid when body effect is included. Note that if $\beta_n = \beta_p$ the second term on the right hand side of the expression disappears and the voltage across the capacitor at the instant of switching is constant and independent of current. Experimental results show that $V_{CAP}$ increased in a nonlinear fashion with current. Therefore it was reasonable to suspect that $\beta_n \neq \beta_p$. Another possible reason for the nonlinearity, switching delays, are not suspected since operation frequency was quite low. Furthermore, if $\beta$ mismatch was the cause, $V_{CAP}$ should have a square root dependence on current. Experimental data confirms this (Fig. 3.8). All that was now required was to determine why the $\beta$'s were not matched, even though measurements showed that, nominally, the $\beta$'s were equal.

Typically, the parameter $\beta$ is expressed as follows

$$\beta = \frac{\mu C_{ox}}{2} \frac{W}{L} . \qquad (3.78)$$

A more accurate representation is given by [23]

$$\beta_{eff} = \frac{\mu_{eff} C_{ox}}{2\,(1+\delta)} \frac{W}{L} . \qquad (3.79)$$

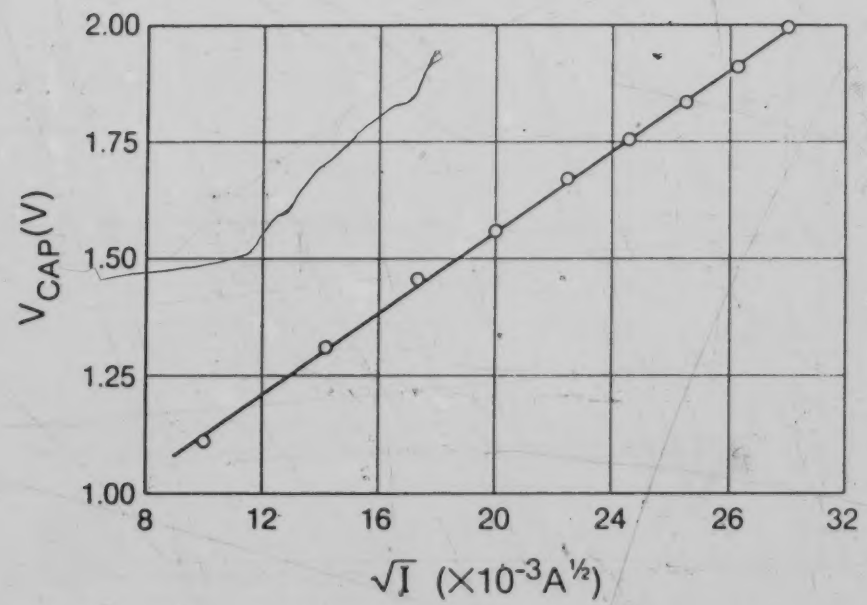


Figure 3.8 Variation of Vcap with I

where:

$$\mu_{eff} \cong \frac{1}{1 + \theta_A(V_{GS}-V_t) + \theta_B V_{SB}} \tag{3.80}$$

and

$$\delta \cong \frac{\gamma}{\sqrt{\phi + V_{SB}}} \tag{3.81}$$

The values of $\theta_A$, $\theta_B$, and $\phi$ are process (fabrication) dependent parameters. The effective $\beta$ of a device is dependent on its operating current (through $V_{GS}$) and on its source to substrate potential ($V_{SB}$) at its operating point, and is not constant as predicted by (3.78). The experimentally measured $\beta$'s used in the previous calculations were determined at a low operating current and with no source-substrate bias. In the circuit, however, the devices operated over a large current range and the NMOS devices M1 and M2 had considerable source to substrate bias.

The dependency of $\beta$ on current and $V_{SB}$ is too complex to be included in the formulations for the frequency, therefore a compromise was used. The devices were remeasured over a large range of currents (50 → 1600 $\mu$A) and for the NMOS, over a range of $V_{SB}$ from 0 to 8 volts. From these results the average value of $\beta$ was found for the desired current range and at the average level of $V_{SB}$ that the devices experience, this value then was used in the theoretical calculations. The level of $V_{SB}$ at which M1 and M2 operate is dependent on current, so an average level of 6 V (determined from the experimental data) was used. For theoretical calculations, an iterative approach to solving the equations has to be used in order to determine the appropriate

level of $V_{SB}$ and $\beta$. A plot of $\beta_n$ versus $V_{SB}$ for the NMOS devices M1 and M2 is shown in Fig. 3.9. Since the $\beta$'s used for the calculations are only average values some error was still expected in the results.

The average values of $\beta$, for $I = 50 \rightarrow 1600$ $\mu$A and with $V_{SB,PMOS} = 0$ and $V_{SB,NMOS} = 6$ V, are $\beta_n \approx 125$ $\mu A/V^2$ and $\beta_p \approx 90$ $\mu A/V^2$. For the NMOS devices the influence of the $\delta$ (3.81) appears to be dominant resulting in an increased value for $\beta$, while for the PMOS devices the mobility degradation (3.80) due to high current effects reduces the effective $\beta$. The frequency characteristic predicted using the corrected values for the $\beta$'s is plotted in Fig. 3.7. The discrepancy between theory and experiment is now less than 10 % over the entire current range. Some systematic error in the frequency/current dependence remains and is probably a result of using a constant value for the $\beta$'s and not the appropriate dependence on current and source substrate voltage, plus, switching delays may begin to deteriorate the linearity at the higher frequencies.

A final check that the difference in $\beta$'s is the real cause of the discrepancy between experiment and theory can be obtained by looking at the slope of the dependence of $V_{CAP}$ on the $\sqrt{I}$. From (3.19) the slope can be found to be

$$\frac{d\,V_{CAP}}{d\,\sqrt{I}} = \sqrt{2}\left[\frac{1}{\sqrt{\beta_p}} - \frac{1}{\sqrt{\beta_n}}\right] \qquad (3.82)$$

and gives a value for the slope of approximately 22 V/$\mu A^2$. The experimentally determined value for the slope is $\approx$ 20 V/$\mu A^2$ (Fig. 3.8). This indicates that, indeed, a large part of the intial

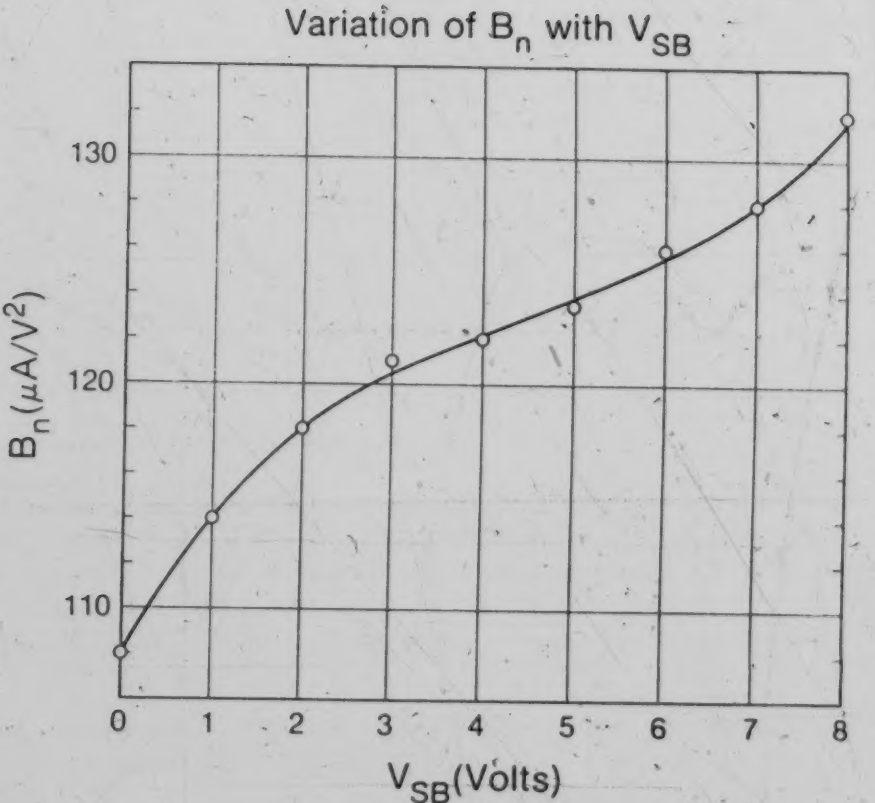


Figure 3.9 Variation of Bn with Vsb

error in calculating the frequency was a result of the inappropriate values for the $\beta$'s.

Some typical waveforms measured at the source and gate of M1 are shown in Fig. 3.10. The rounded corners on the gate waveforms just before each transition correspond to the region where the circuit is in linear operation.

## 3.6 Conclusion

The ability to adequately predict the nonlinear frequency characteristic of the SCM with active/resistive loads indicates that the basic operation and theory of the oscillator is understood. The theory indicates that linear control of frequency requires well-matched load (M3, M4) and threshold (M1, M2) devices , especially in terms of the gain coeffiecient $\beta$. Practical experience, as witnessed from Experiment 3.2, indicates that adequate matching cannot easily be achieved for devices of opposite polarity (PMOS and NMOS) operating over a large current range and experiencing the body effect. An all-NMOS circuit, with NMOS loads, would likely provide better matching between the load and threshold devices provided that no body effect is present. But, in general, the SCM is very dependent upon device parameters to achieve a linear frequency characteristic with current. As a result, the SCM is not very suitable for use as a CCO. Reproducibilty of linearity would be a major concern in any application.

Due to its unsuitability for CCO applications such questions as frequency stability with temperature, power supply and noise were not

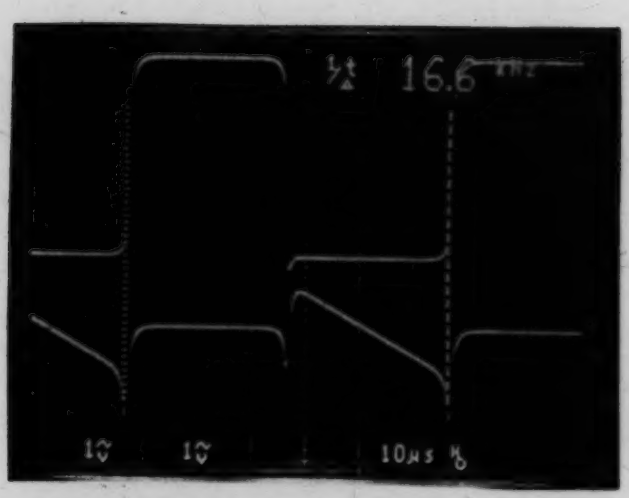


(a) I = 200 uA,

(b) I = 1500 uA

Figure 3.10 Gate (Upper) and Source (Lower) Waveforms

addressed for the SCM.

Although the SCM is not a good candidate for CCO applications, some important lessons can be learned and applied to future designs of CMOS CCOs. One major problem of the SCM is that the threshold voltage which determines the switching point is dependent on the level of the charge/discharge current. Since the frequency of oscillation is dependent upon the ratio of the charge/discharge current and the threshold voltage, a nonlinear control characteristic results. This problem can be alleviated by separating the threshold circuit from that which controls the charging current to the capacitor. The threshold circuit should sense the voltage on the capacitor whereas the charge circuit should provide the appropriate current level and direction to the capacitor. In this way the frequency of oscillation can be varied by the charge/discharge current without affecting the threshold levels. Better linearity of the frequency characteristic with current should result. The idea of using separate control/threshold circuits is by no means new and has been used in such circuits as the Kukielka, Wakayama, and 4046 type multivibrators as discussed in Chapter 2. The SCM shows just how important it is to separate the two functions, thereby allowing each function to be optimized independently. What the SCM gained in simplicity by combining the threshold/charge circuit into just four transistors, it lost in performance.

Heavy reliance on device matching to achieve adequate performance as was required by the SCM is a tenuous proposition at best. Nominally the devices used in Experiment 3.2 were matched, but varying

operating conditions such as current levels and source substrate voltage resulted in mismatches. Since the performance of the circuit required good matching to achieve the desired linearity, the performance was severely degraded by relatively small mismatches. Ideally, circuit performance should be made largely independent of the device parameters.

For applications where good linearity is not required, the SCM provides an extremly simple and compact circuit. Four transistors M1 → M4 provide the core of the circuit. The relatively small signal swings throughout the circuit should be benefical if high frequency operation is required.

## 4.0 Piskarev Multivibrator

### 4.1 Introduction

A major flaw of the source coupled multivibrator is the dependence of the threshold circuit's hysteresis voltage on the level of the capacitor charging current. This results in a nonlinear current versus frequency characteristic. A new current controlled multivibrator is proposed in which the hysteresis voltage is kept independent of the charging current by using strict subdivision of the threshold and charge circuits. The proposed CCO has the following features: independence of the hysteresis voltage on the charge/discharge current and power supply voltage $V_{CC}$, small signal swings are maintained throughout to help minimize switching delays, and a relatively simple design.

### 4.2 Basic Multivibrator

The threshold circuit is the most important element of any multivibrator. The proposed multivibrator's threshold circuit is based on the CMOS implementation of a circuit recently proposed and used by Piskarev [24] in a bipolar multivibrator (which was not current controlled). As a result, the proposed multivibrator will be referred to throughout this work as the Piskarev multivibrator. The Piskarev-type threshold circuit was chosen primarily for two reasons, both related to speed: first, the output of the circuit can provide a relatively small swing and, second, the circuit is very simple which helps to minimize switching delays.

The basic Piskarev multivibrator is shown in Fig. 4.1(a). The

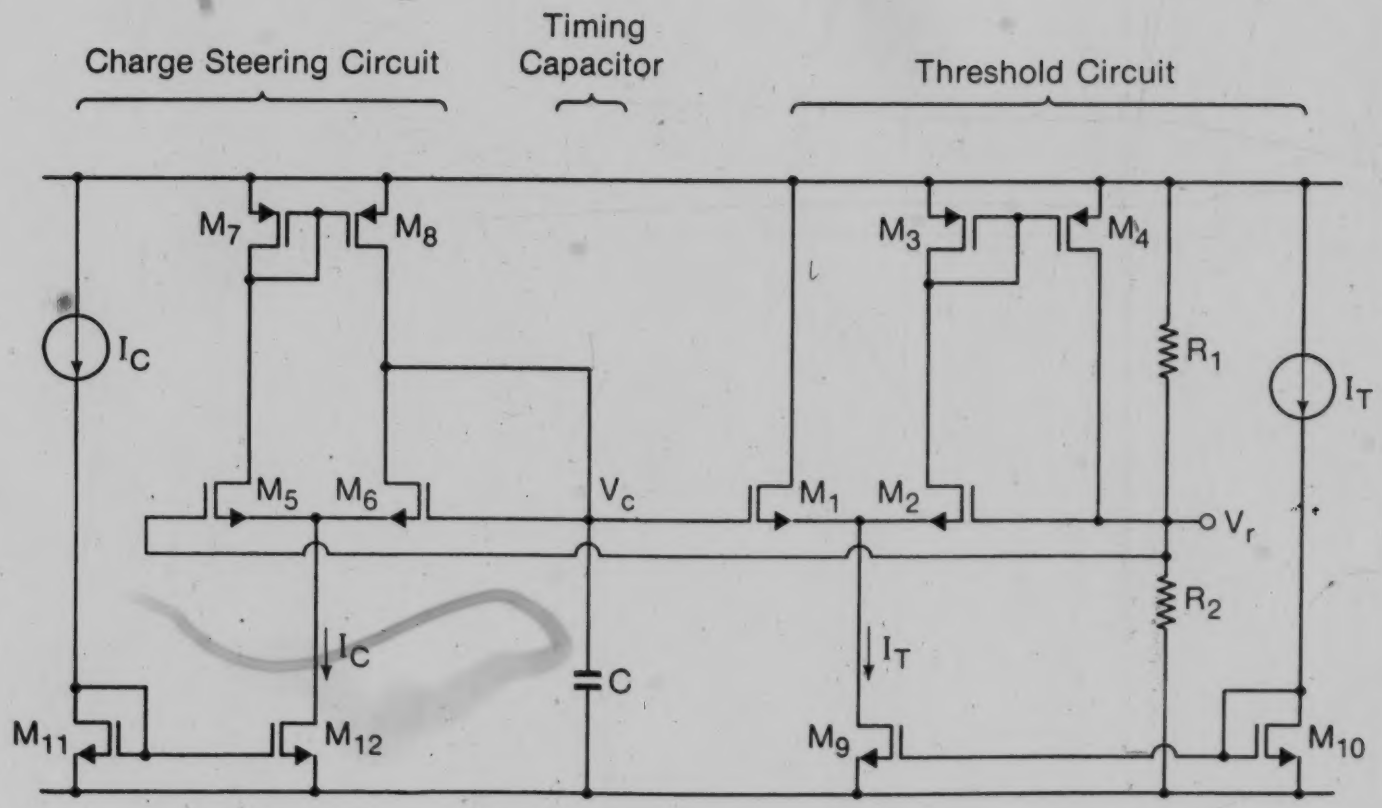


Figure 4.1 Basic Piskarev Multivibrator

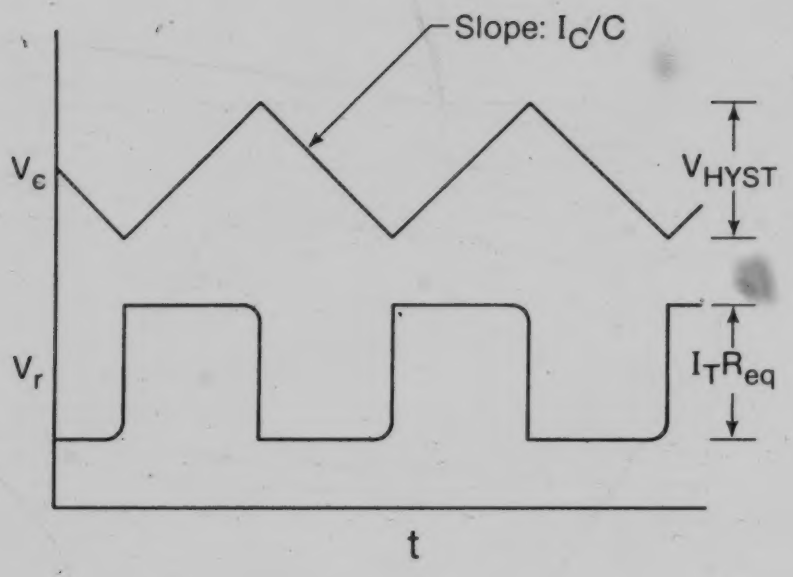


**Figure 4.1(b) Typical Waveforms for Piskarev Multivibrator**

threshold circuit is composed of transistors M1 to M4 and resistors $R_1$ and $R_2$. Transistors M5 to M8 form the charging circuit, and biasing is provided for the threshold and charge circuits by M9-M10 and M11-M12 respectively. The frequency of oscillation is determined by the timing capacitor $C$.

The charging circuit is a departure from tradition. Typically, in CMOS multivibrators, the direction of the charge/discharge current to the timing capacitor is controlled by conventional CMOS switches [9] (Fig. 4.2). In the Piskarev multivibrator current steering is provided by a differential pair (Fig. 4.3). To switch a current using a differential pair a differential input signal of

$$|V_{switch}| = \sqrt{\frac{I}{\beta}} \qquad (4.1)$$

is required [34]. Conventional CMOS switches are typically operated with input signals that swing rail to rail. The use of the differential pair current switch is important because it allows the signal swings throughout the multivibrator to remain relatively small, thereby reducing the switching delays.

Initially, after application of $V_{CC}$, the voltage across the capacitor, $V_C$, is zero and the voltage at the center of the resistive divider, $V_R$, is greater than zero. As a result M1 is *OFF* and M2 is *ON*. The current mirror formed by M3-M4 provides positive feedback to the gate of M2 and the voltage at $V_R$ soon comes to rest at the quasistable level of

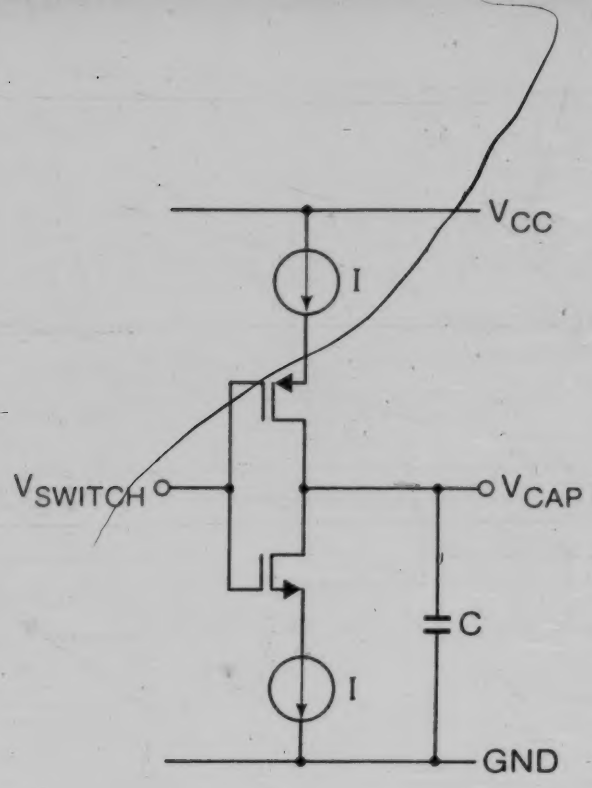


Figure 4.2 Typical CMOS Current Switch

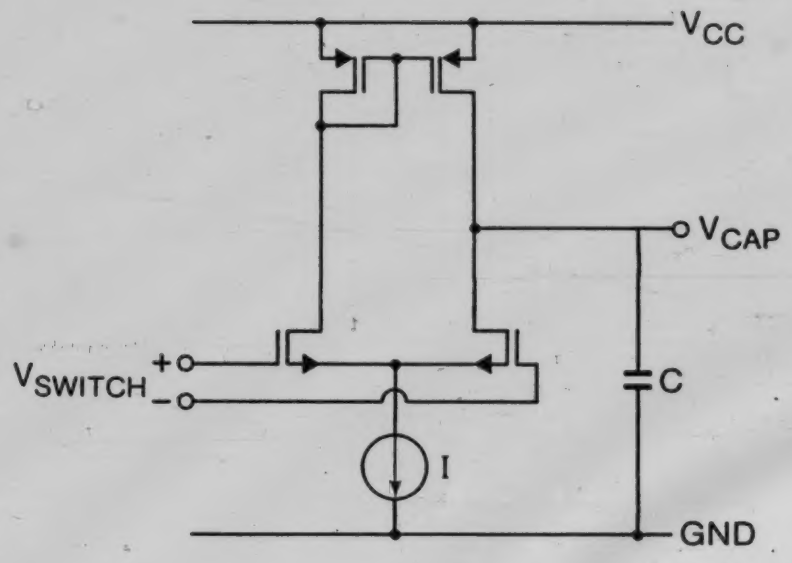


Figure 4.3 Differential Pair Current Switch

$$V_{R,HIGH} = V_{CC}\frac{R_2}{R_1+R_2} + I_T\frac{R_1R_2}{R_1+R_2} = V_{CC}\frac{R_{eq}}{R_1} + I_T R_{eq} \qquad (4.2)$$

where

$$R_{eq} = \frac{R_1R_2}{R_1+R_2} \qquad (4.3)$$

The charge and threshold differential pairs have their gates connected in parallel, therefore M5 is *OFF*, and M6 is *ON*. The capacitor is charged by a constant current $I_C$ and $V_C$ increases linearly with a slope of $I_C/C$ towards $V_{CC}$. As $V_C$ approaches the upper threshold $V_{TH,HIGH}$ (near $V_{R,HIGH}$), M1 begins to turn *ON* and by the differential action of M1 and M2 the current through M2 ($I_{D2}$) decreases. The decrease of $I_{D2}$ is helped by the positive feedback through the current mirror M3-M4, and the voltage at $V_R$ rapidly decreases to a level

$$V_{R,LOW} = V_{CC}\frac{R_{eq}}{R_1} \qquad (4.4)$$

The direction of the charging current into the capacitor is reversed and the capacitor voltage decreases linearly towards *GND*. As $V_C$ nears the lower threshold $V_{TH,LOW}$ (near $V_{R,LOW}$) the current through M2 begins to increase and due to positive feedback $V_R$ rapidly increases to $V_{R,HIGH}$. One cycle is complete and the circuit begins astable operation with a frequency of

$$f_o = \frac{I_C}{2\,C\,(V_{TH,HIGH} - V_{TH,LOW})} \qquad (4.5)$$

Later, it will be shown that the threshold voltage levels are

independent of $I_C$. Linear control of frequency can therefore be obtained through the input variable $I_C$.

## 4.3 Threshold Circuit

A detailed analysis of the threshold circuit (Fig. 4.1) will now be performed. First the upper and lower threshold points will be determined by applying the condition that at the point of regenerative switching the loop gain is equal to +1. The small signal equivalent of the threshold circuit is shown in Fig. 4.4(a) and reduces to the circuit in Fig. 4.4(b). Note that the equivalent circuit shown in Fig. 4.4(b) is identical to that of the source coupled multivibrator (Fig. 3.3) if $Z_1 = R_{eq}$ and $Z_2 = 0$. The similarity is expected since both circuits behave as a differential pair with positive feedback during the instant of transition. Therefore, the derivation of the condition for $A_{LOOP} = 1$ for the SCM can be directly applied to the Piskarev multivibrator. Hence, the condition for regenerative switching of the Piskarev threshold circuit is given by (3.40):

$$\frac{1}{g_{m1}} + \frac{1}{g_{m2}} = R_{eq} \quad . \tag{4.6}$$

From (4.6) the currents in M1 and M2 can be determined at the threshold points. At the lower threshold the currents are:

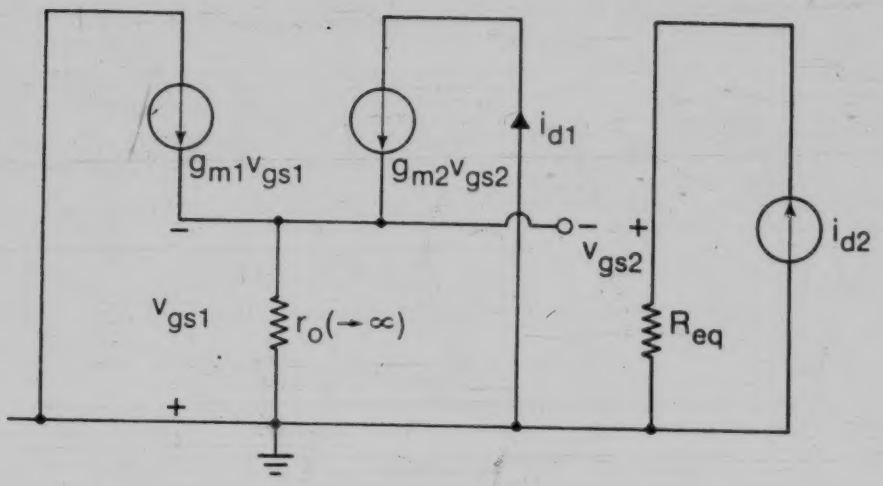


Figure 4.4(a) Small Signal Equivalent Circuit for Loop Gain Calculation

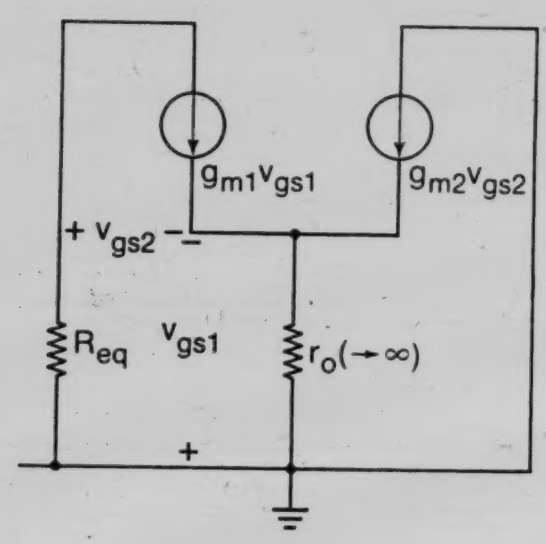


**Figure 4.4(b) Simplified Small Signal Equivalent Circuit**

$$I_{D1,L} = \frac{I_T}{2}\left[1 + \sqrt{1 - 4\,m_{th}^2}\right] \tag{4.7}$$

$$I_{D2,L} = \frac{I_T}{2}\left[1 - \sqrt{1 - 4\,m_{th}^2}\right] \tag{4.8}$$

and, at the upper threshold,

$$I_{D1,H} = \frac{I_T}{2}\left[1 - \sqrt{1 - 4\,m_{th}^2}\right] \tag{4.9}$$

$$I_{D2,H} = \frac{I_T}{2}\left[1 + \sqrt{1 - 4\,m_{th}^2}\right] \tag{4.10}$$

where:

$$m_{th} = \frac{1}{\sqrt{1 + 4\,R_{eq}^2\,\beta_{nT}\,I_T} - 1} \tag{4.11}$$

where $\beta_{nT}$ is the gain coefficient of the devices in the threshold circuit differential pair (Fig. 4.1(a)).

Once the currents through M1 and M2 at the switching points are determined, the thresholds can be easily calculated. The lower threshold is given by:

$$V_{TH,LOW} = V_{CC}\frac{R_{eq}}{R_1} + I_{D2,L}\,R_{eq} \cdots$$

$$- \left[V_{tn2} + \sqrt{\frac{I_{D2,L}}{\beta_{nT}}}\right] + \left[V_{tn1} + \sqrt{\frac{I_{D1,L}}{\beta_{nT}}}\right] . \tag{4.12}$$

The sources of M1 and M2 are common, therefore:

$$V_{tn1} = V_{tn2} \tag{4.13}$$

and (4.12) simplifies to:

$$V_{TH,LOW} = V_{CC}\frac{R_{eq}}{R_1} + I_{D2,L}R_{eq} - \sqrt{\frac{I_{D2,L}}{\beta_{nT}}} + \sqrt{\frac{I_{D1,L}}{\beta_{nT}}} \tag{4.14}$$

Similarly, the upper threshold can be determined to be:

$$V_{TH,HIGH} = V_{CC}\frac{R_{eq}}{R_1} + I_{D2,H}R_{eq} - \sqrt{\frac{I_{D2,H}}{\beta_{nT}}} + \sqrt{\frac{I_{D1,H}}{\beta_{nT}}} \tag{4.15}$$

The hysteresis voltage of the threshold circuit is:

$$V_{HYST} = V_{TH,HIGH} - V_{TH,LOW} \tag{4.16}$$

and, combining the above equations yields:

$$V_{HYST} = R_{eq}\frac{I_T}{2}\left[\left(1+\sqrt{1-4m_{th}^2}\right) - \frac{I_T}{2}\left(1+\sqrt{1-4m_{th}^2}\right)\right] \cdots$$

$$- 2\sqrt{\frac{I_T}{2\,\beta_{nT}}}\left(\sqrt{1-\sqrt{1-4m_{th}^2}} - \sqrt{1+\sqrt{1-4m_{th}^2}}\right). \tag{4.17}$$

If $m_{th} \ll 1/2$, then the hysteresis voltage can be approximated as

$$V_{HYST} \approx R_{eq}I_T - 2\sqrt{\frac{I_T}{\beta_{nT}}}. \tag{4.18}$$

## 4.4 Complete Multivibrator

Once the hysteresis voltage of the threshold circuit is determined, the frequency of oscillation follows quickly. For this derivation, the following assumptions are made:

(1) the capacitor charging current is considered to be constant during each half cycle, i.e. the switching time is much less than the period,

(2) the charge current is entirely switched by the threshold circuit which requires that

$$I_C \leq I_T \frac{\beta_{nC}}{\beta_{nT}} \quad , \tag{4.19}$$

where $\beta_{nC}$ is the gain coefficient of the devices in the charge steering differential pair (Fig. 4.1(a))

(3) the swing of $V_R$ is large enough to ensure proper switching of the current within the threshold circuit; this requires that

$$R_{eq} \geq \sqrt{\frac{1}{I_T \beta_{nT}}} \quad . \tag{4.20}$$

If these conditions are satisfied, then the frequency of oscillation is given by

$$f_o = \frac{I_C}{2\, C\, V_{HYST}} \tag{4.21}$$

where $V_{HYST}$ is given by (4.17). If $m_{th} < 1/2$, then the frequency can

be approximated as

$$f_o \approx \frac{I_C}{2\,C\left[R_{eq}\,I_T - 2\sqrt{\frac{I_T}{\beta_{nT}}}\right]} \qquad (4.22)$$

Since the denominator of (4.22) (and 4.21) is independent of $I_C$, linear control of frequency can be achieved through the variable $I_C$.

## 4.5 Frequency Stability

Ideally, for a constant input current, the frequency of a CCO is perfectly stable. In reality the output frequency of the multivibrator experiences both short and long term instabilities, the former called jitter and the latter drift. The importance of each type of instability depends upon the application. A VCO used in a PLL with a narrow BW loop filter requires good long term stability to ensure that the center frequency does not drift out of the lock range of the input signal. For clock recovery circuits, short term stability is important, since jitter imposed on the recovered clock increases the bit error rate of the regenerated data.

Short term frequency instabilities of multivibrators are caused primarily by noise modulating the threshold levels. Drift, or long term instability, can be the result of many factors such as temperature variations, slow variations in the power supply voltage, and component aging.

### 4.5.1 Thermal Stability

The behaviour of electrons varies with temperature [21]. As a result all electronic components have temperature dependent behaviour. In CCOs the variation of device parameters with temperature results in frequency drift. Temperature can be considered to be another input variable to the CCO, in a sense making it a temperature controlled oscillator. Clever circuit design can reduce the temperature coefficient of an oscillator but cannot eliminate it. From (4.21 and 4.18), assuming $m_{th} \ll 1/2$, the sensitivity of the Piskarev multivibrator's frequency to temperature is found to be given by:

$$\frac{1}{f_o}\frac{df_o}{dT} = \frac{d\left[\dfrac{I_C}{2\,C\,V_{HYST}}\right]}{dT}$$

$$\approx \frac{1}{I_C}\frac{\partial I_C}{\partial T} - \frac{1}{C}\frac{\partial C}{\partial T} - \frac{1}{V_{HYST}}\left[ I_T R_{eq}\left( \frac{1}{R_{eq}}\frac{\partial R_{eq}}{\partial T} + \frac{1}{I_T}\frac{\partial I_T}{\partial T}\right) \cdots \right.$$

$$\left. + \sqrt{\frac{I_T}{\beta_n}}\left( \frac{1}{I_T}\frac{\partial I_T}{\partial T} - \frac{1}{\beta_n}\frac{\partial \beta_n}{\partial T}\right)\right] \qquad (4.23)$$

where (from [23])

$$\frac{\partial \beta_n}{\partial T} = \frac{\partial}{\partial T}\left[\frac{\mu C_{ox}}{2}\frac{W}{L}\right] \approx \frac{C_{ox}}{2}\frac{W}{L}\left[\frac{\mu(T_r)\ (-k)}{T_r}\ T^{-(k+1)}\right] \tag{4.24}$$

$T$ = absolute temperature (in $^{\circ}K$)

$T_r$ = room temperature (in $^{\circ}K$)

$k$ = process dependent parameter between 1.5 and 2

As seen from the above expression, a low temperature coefficient for frequency can only be achieved through the minimization (or cancelation) of each $\partial/\partial T$ term. This cannot be achieved easily for a totally integrated CCO since components such as resistors typically have very poor TCs, i.e. from 1500 to 8000 ppm/°C for poly and p-well resistors [25] respectively. Capacitors have lower TCs, with TCs of about 25 ppm/°C being typical for a double poly capacitor [25]. So, if good thermal stability is required, external threshold setting resistors ($R_{eq}$) should be used. The influence of the temperature dependence of $\beta$ can only be minimized by reducing the contribution of the term $(I_T/\beta_T)^{1/2}$ to the overall hysteresis voltage, this will be discussed in Section 4.10. Finally, the threshold current $I_T$ should be generated in a thermally stable fashion. See Section 4.10 for futher discussion on methods of reducing thermal drift.

### 4.5.2 Jitter

The cycle to cycle variation of a multivibrator's period, due to modulation of the effective threshold voltage by noise, is called frequency jitter. The highly nonlinear nature of the multivibrator

makes jitter measurement and analytical analysis difficult [18]. Only some basic guidelines to jitter reduction will be offered.

Jitter results from noise modulating the effective threshold level. One approach to jitter reduction is to reduce the circuit noise using traditional low noise design techniques [34,26]. These techniques rely on the reduction of the noise sources. Another approach to the problem is from a topological point of view. Due to the nonlinear nature of the multivibrator, $V_C$, the capacitor voltage only affects the threshold circuit when it is near a threshold level. Therefore, by increasing the rate at which the capacitor voltage approaches the threshold, less time is spent in the region where it is vulnerable to corruption by noise and jitter is reduced. This is the technique used by Wakayama [12] to achieve a jitter of < 100ppm. For a given frequency, the slope of the capacitor voltage can be increased by increasing $V_{HYST}$. For low jitter CCOs both techniques should be applied.

Another source of frequency jitter is from rapid variations in the supply voltage due to noise on the supply lines or poor regulation. To the first order, the Piskarev multivibrator is immune to power supply variations since the hysteresis voltage in independent of $V_{CC}$. But second order effects such as the finite output impedance of the current sources and mirrors, plus the resistive divider formed by $R_1$, $R_2$ allow supply variations to enter the circuit and contribute extra noise to the circuit. The most effective means of reducing the effects of supply variations is external to the circuit and involves ensuring adequate decoupling of supply lines, separation of digital

and analog supplies, and providing good supply regulation.

## 4.6 Choice of Hysteresis Voltage

The choice of the hysteresis voltage, $V_{HYST}$, is a compromise between minimizing switching delays and improving stability. For a given frequency, jitter can be reduced by increasing $V_{HYST}$ so that the rate at which $V_C$ approaches the threshold is increased, this requires that $V_{HYST}$ be made as large as possible. Switching delays depend largely on the amount of voltage the parasitic nodal capacitance must be charged/discharged through (plus the amount of charging current available). Reduced delays dictate that small signal swings be used throughout the circuit, therefore $V_{HYST}$ should be kept small. The optimal balance of stability and speed will be determined by the intended application of the CCO.

## 4.7 Modifications

Applications of CCOs are many and varied; each places different emphasis of the various criteria such as linearity, range, stability, and size; no one CCO design is, therefore, the best for all applications. Some modifications to the basic Piskarev multivibrator will now be presented that allow it to be fine-tuned for its intended use.

### 4.7.1 Buffer Stage

An important modification to the basic Piskarev multivibrator is the addition of a buffer stage to the threshold circuit to reduce loading of the output on this critical stage. A simple buffer which

makes full use of the circuit topology is shown in Fig. 4.5 and consists of M13 to M17. If additional drive capability is required, the output of this stage can be used to drive further inverter stages until the desired drive capability is achieved. By proper design of the inverters' $W/L$ ratios, i.e. the ratio should grow by a factor of e ($\approx 2.7$) between stages, increased drive capability can be achieved with minimum delay [27].

The addition of the buffer stage increases the capacitive loading at the drain of M2 resulting in increased switching delays for the threshold circuit. To reduce the capacitive loading, M16 should be kept relatively small compared to M3 and any additional drive required for the ouput should be obtained through additional inverter stages.

The output of the buffer stage swings from rail to rail, but since it is not in the signal path of the threshold/charge circuit, the increased switching delays due to the large swings will not be detrimental to the circuit's performance (maximum output frequency is, however, limited by the buffer delays).

### 4.7.2 Using Buffer Output to Control Charge Circuit

In the basic Piskarev multivibrator the maximum charge current is limited by the requirement that (from 4.19)

$$I_C \leq I_T \frac{\beta_{nC}}{\beta_{nT}} \quad . \tag{4.25}$$

This condition must be met to ensure that the switching voltage across the threshold differential pair is adequate to completely switch the charge circuit differential pair.

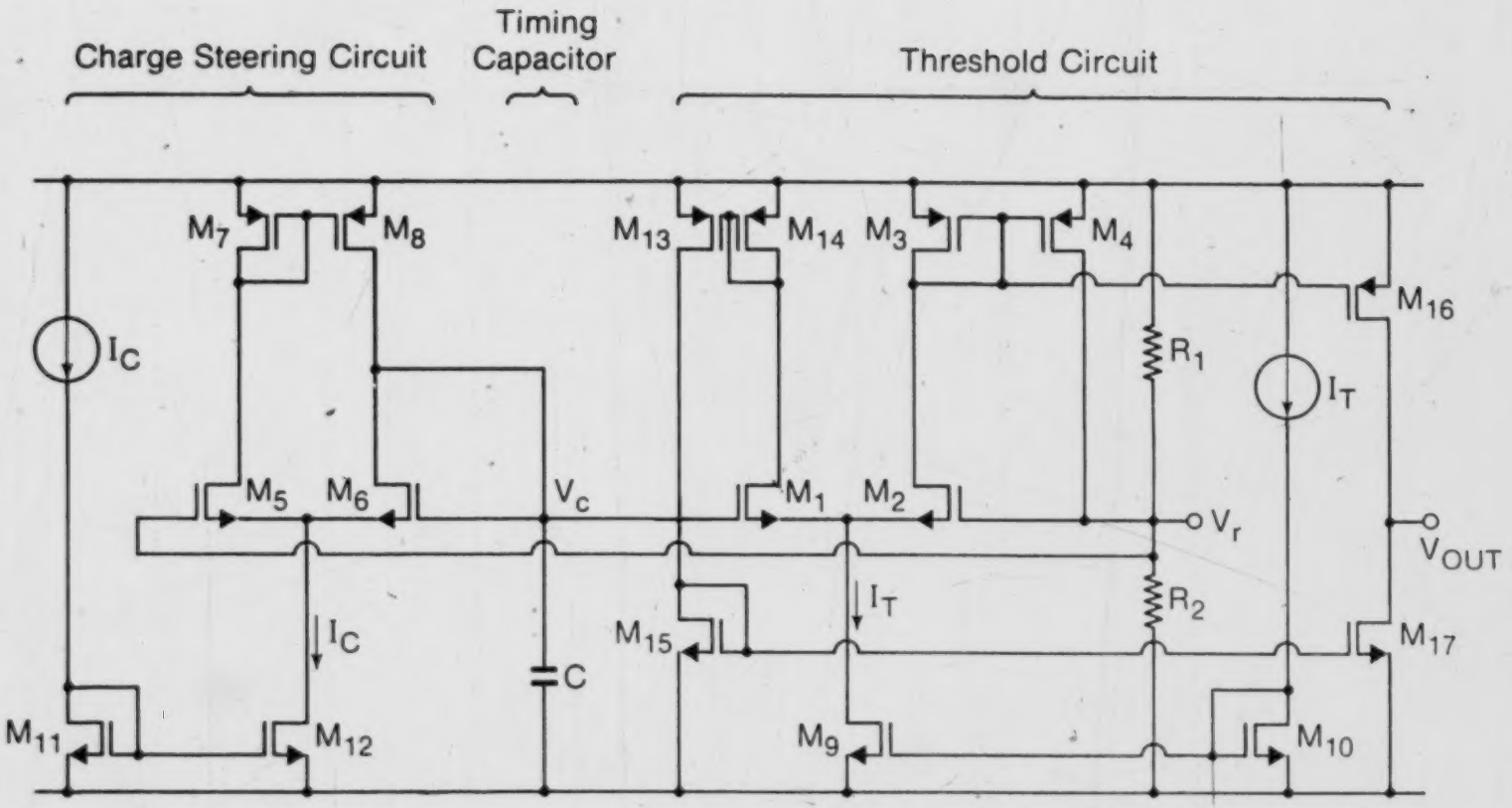


Figure 4.5 Piskarev Multivibrator with Buffer Stage

Increased range for the charge current can be obtained by moving the gate of M5 from M2 to the output of the buffer stage (drain of M17) as shown in Fig. 4.6. This provides a greater voltage swing with which to switch the charge circuit differential pair. Now, the entire charging current can be switched if the following expression is satisfied:

$$\beta_{nC} ( V_{GND} + V_{TH,LOW} )^2 \geq I_C \leq \beta_{nC} ( V_{CC} - V_{TH,HIGH} )^2 \quad . \qquad (4.26)$$

A further increase in the charge current range can be obtained by using a buffer stage, which inverts the output signal, and using this to drive the gate of M5, while the gate of M6 is driven by the capacitor voltage. The condition for full switching of the charge differential pair now becomes:

$$\beta_{nC} ( V_{GND} + V_{TH,HIGH} )^2 \geq I_C \leq \beta_{nC} ( V_{CC} - V_{TH,LOW} )^2 \quad . \qquad (4.27)$$

It should always be checked that the circuits are still operating in pinchoff at the desired current level.

The use of the buffer output to drive the charge differential pair introduces additional switching delays which will degrade the high frequency performance. The current control range, however, will be increased.

### 4.7.3 Single Supply / Split Supply Operation

The Piskarev multivibrator can be operated with either a single or split supply. The choice is often determined by the availability of split supplies in the intended application. If split supplies are

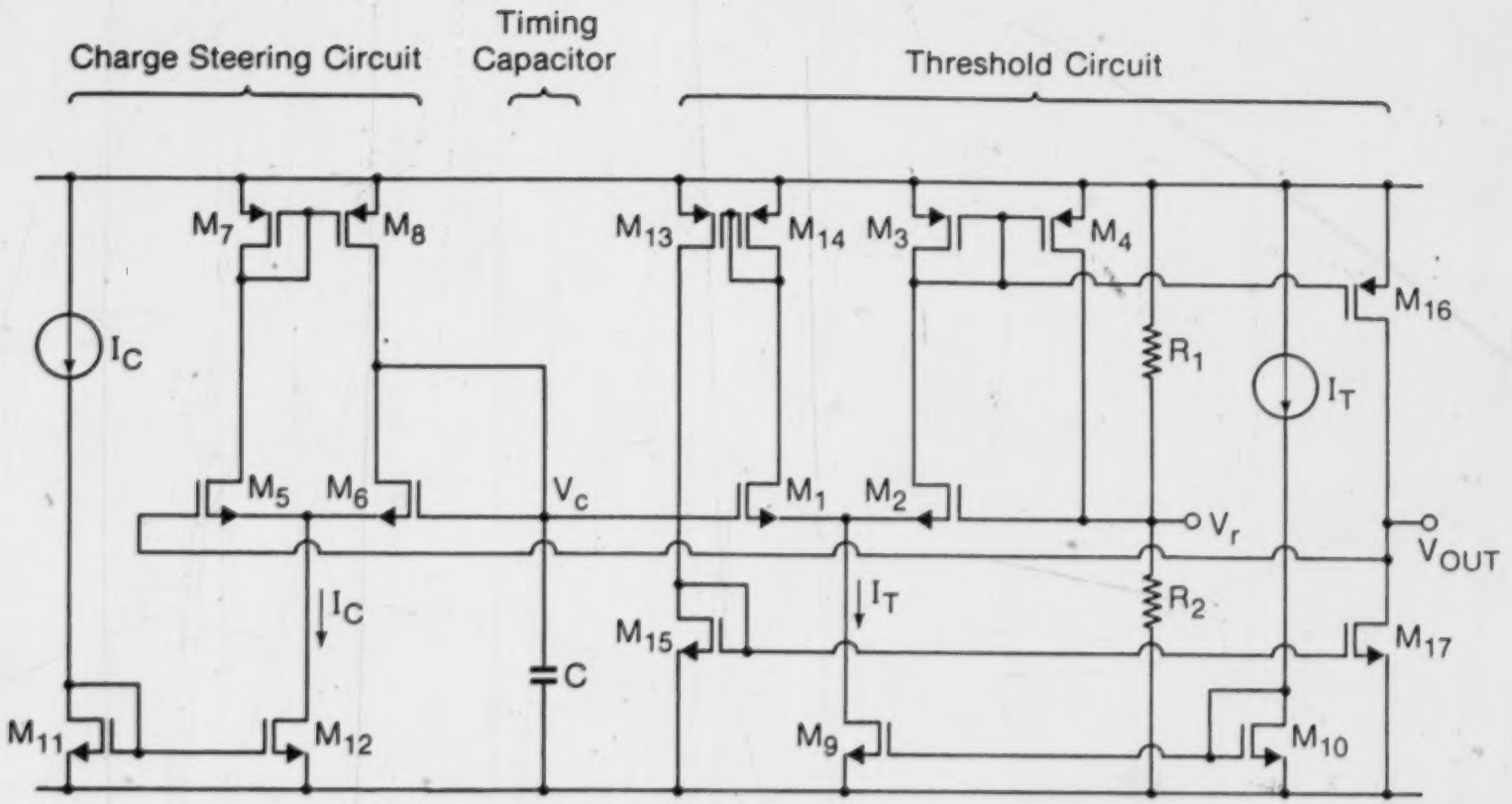


Figure 4.6 Piskarev Multivibrator with
Buffer Stage Controlling Charge Steering Circuit

available, then the chip area required to implement the threshold resistors can be reduced.

The only modification to the basic Piskarev multivibrator for split supply operation is the replacement of the resistive divider network formed by $R_1, R_2$ with a single resistor of value $R_{SS} = R_{eq}$ connected to *GND* (Fig. 4.7). Maintaining the same signal swing at $V_r$, and assuming constant $I_T$, the total resistance required by the split supply circuit will be reduced by a factor of four compared to the single supply version. A four fold decrease in the chip area required for fabricating the required resistors is achieved by using of split supplies. The savings in area can be significant. Consider fabricating a 1kΩ resistor using 50Ω/square diffusion [25], this would require 20 squares or an area of 200x10 $\mu^2$ if 10$\mu$ squares are used.

If the total area consumed in fabricating the resistors is held constant, then for the same $V_r$ swing, the threshold bias current, $I_T$, can be reduced by a factor of four. Such a measure reduces power consumption and increases the hysteresis voltage (for the same $V_r$ swing) which, in turn, helps reduce jitter.

### 4.7.4 Current Mirror Gain

Small switching delays dictate that the swing of $V_r$ be kept small, whereas low jitter requires $V_{HYST}$ to be large. In the basic Piskarev multivibrator the hysteresis voltage is given approximately by

$$V_{HYST} \approx R_{eq} I_T - 2\sqrt{\frac{I_T}{\beta_{nT}}} \qquad (4.28)$$

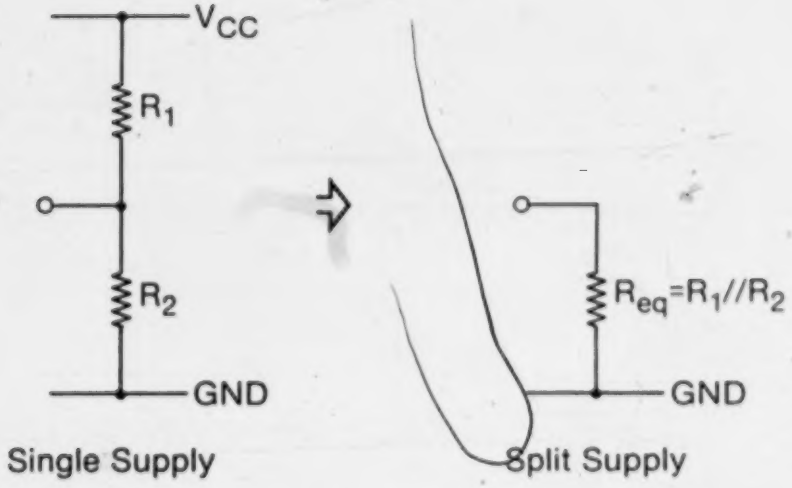


**Figure 4.7 Threshold Setting Resistor(s) Configurations for Single & Split Supply Operation**

and the swing of $V_r$ is given by

$$V_{r,swing} = R_{eq} I_T \tag{4.29}$$

In order to increase the hysteresis voltage without increasing the swing of $V_r$ the gain coefficient $\beta_{nT}$ of the threshold differential pair could be increased, which means increased device size for M1 and M2. Alternatively, the threshold current, $I_T$ , can be reduced while increasing $R_{eq}$. This increases the area required for fabricating the resistors.

An alternate method is to provide current gain in the current mirror formed by M3 and M4. Let

$$\left[\frac{W}{L}\right]_4 = A\left[\frac{W}{L}\right]_3 \tag{4.30}$$

where $A$ is the current gain. Now, the effective threshold current through the differential pair can be reduced by a factor of $A$ thereby increasing the hysteresis voltage without affecting the swing at $V_r$. Since the size of only one device is changed, the area increase will typically be less than that required to increase the $\beta$ of M1 and M2, or the size of the resistors. The decrease in $I_T$ will reduce the control range, unless the charge differential pair is driven by the buffer output as discussed previously.

Increasing the size of M4 will increase the capacitive loading on the drain of M2 and so some increase in switching delay is expected. The benefit of decreased jitter should outweigh the increased delay for most applications.

### 4.7.5 Voltage Gain at Input to Threshold Circuit

Another method for increasing the hysteresis voltage without increasing the swing at $V_r$ is to provide voltage gain between the timing capacitor and the input to the threshold circuit. This is illustrated in Fig. 4.8 using a comparator. The hysteresis voltage will be given by

$$V_{HYST} \approx R_{eq} I_T - \frac{2\sqrt{I_T / \beta_{nT}}}{A_v} \approx R_{eq} I_T \qquad (4.31)$$

if $A_v$ (the voltage gain of the comparator) is large. The hysteresis voltage is equal to the swing of $V_r$. Unfortunately, the addition of the comparator in the threshold signal path introduces an additional switching delay due to its large signal swings and the whole point of using reduced signal swings to improve frequency performance is defeated.

## 4.8 Experimental Verification

The basic Piskarev multivibrator was breadboarded using the MO415 CMOS transistor arrays from Ferranti Interdesign [14]. First, the threshold circuit was separated from the rest of the multivibrator and the hysteresis voltage was measured as a function of $R_{eq}$. Then the entire circuit was reconnected and the frequency as a function of current was measured. This provided experimental verification of the basic theory and concepts of the Piskarev multivibrator. All measurements were carried out at low frequencies to minimize the

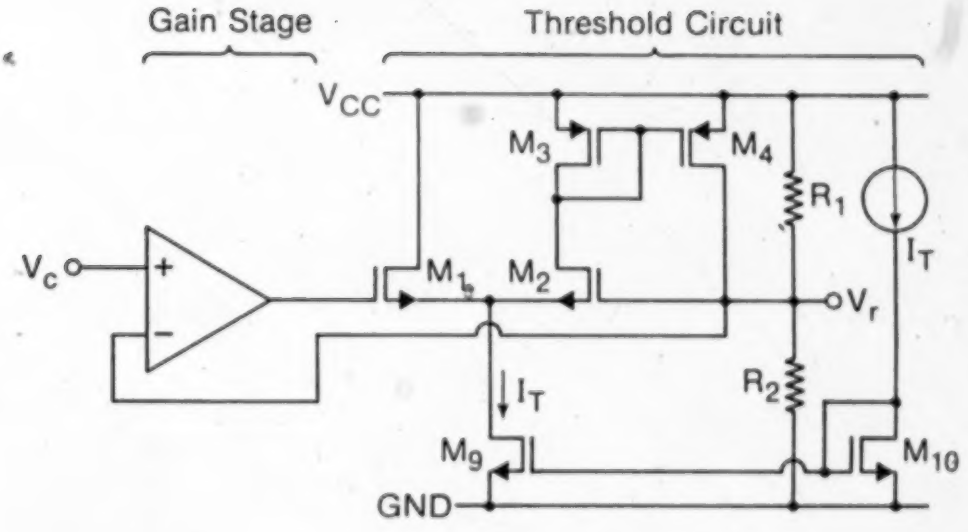


Figure 4.8 Gain Stage at Input of Threshold Circuit

effect of switching delays.

Breadboarding with discrete devices does not provide a true representation of the capabilities of a wholly integrated Piskarev multivibrator. The use of discrete devices and the plug-in type breadboard results in excessive parastic capacitances which degrade the frequency performance. To provide a clearer picture of the obtainable performance, SPICE [28] simulations were used to evaluate high frequency operation. Two areas of interest were investigated: (1) the influence on high frequency performance of using the buffer stage to control the charge circuit, and (2) the range of frequency control that is possible with this configuration.

The Piskarev multivibrator is intended for integrated circuit applications and verification of its performance in this form would be desirable. CMOS fabrication facilities are available to the student through the Canadian Microelectronics Corporation (CMC). With this in mind, the core of the multivibrator, consisting of the threshold and charge circuits (see appendix 2) but not including the bias generation circuits nor the R's and C, has been designed, layed out, and submitted for fabrication in the CMOS1B [29] process available through the CMC. The SPICE simulations are based upon these designs and this should provide a check of the simulation accuracy. Unfortunately, due to time constraints, these devices will not be available for testing in time for inclusion in this work.

### 4.8.1 Breadboard Verification: Experiments 4.1, 4.2a, 4.2b

The most important portion of the theory deals with the prediction of the hysteresis voltage. To test the accuracy of the

predicted hysteresis voltage the threshold circuit of the basic Piskarev multivibrator (Fig. 4.9) was constructed using the CMOS transitors array available from Ferranti Interdesign. Discrete resistors and capacitors were used to allow increased flexibilty in the experimental conditions. The device parameters for the experimental circuit are found in Table 4.1.

The threshold parameter $m_{th}$ (4.11) has a strong influence on the hysteresis voltage and can be varied through $R_{eq}$. The hysteresis voltage was measured (Exp. 4.1) for a range of $R_{eq}$ = 18 → 30kΩ (with $I_T$ and $\beta_{nT}$ held constant) and compared with the values predicted by (4.21). This range of $R_{eq}$ corresponds to a variation of $m_{th}$ = 1/2 → 0 (the entire valid range for $m_{th}$). Good coincidence between the experimental and theoretical results is obtained over the entire range (Fig. 4.10). For oscillations to occur, the hysteresis voltage must be greater then zero, or $m_{th} < 1/2$ (see 4.11) so the minimum value for $R_{eq}$ is set by the requirement

$$R_{eq} \geq \sqrt{\frac{2}{I_T \beta_{nT}}} \tag{4.32}$$

or more generally

$$R_{eq}^2 I_T \beta_{nT} \geq 2 \quad . \tag{4.33}$$

For the test circuit $R_{eq,min}$ = 14 kΩ, which corresponds roughly with the x axis intercept (≈15 kΩ) of the hysteresis voltage versus $R_{eq}$ graph in Fig. 4.10. Accurate prediction of the hysteresis voltage is possible over the entire range of $m_{th}$, indicating that the operation

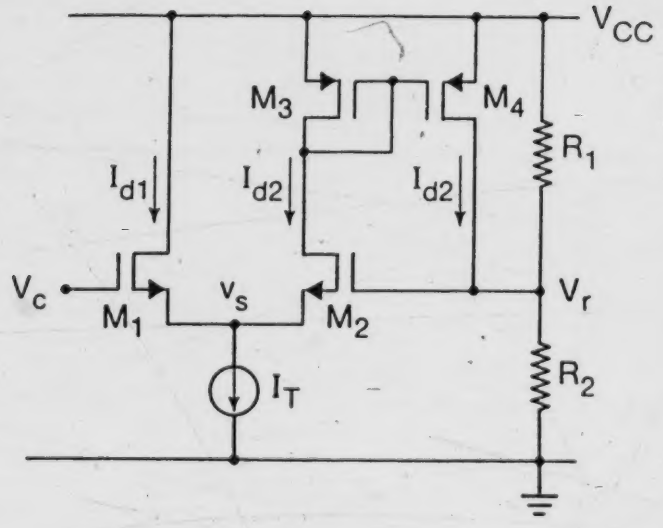


Figure 4.9 Threshold Circuit

| | NMOS | PMOS |
|---|---|---|
| W/L | 310/24 | 580/24 |
| $\beta^*$ ($\mu A/V^2$) | 110 | 110 |
| $V_t$ (V) | 1.25 | 0.9 |
| $\gamma$ ($V^{1/2}$) | 1.8 | - |
| $\phi_f$ (V) | 0.3 | 0.3 |

* Measured at $|I_D| \approx 50\ \mu A$ and $|V_{SB}| \approx 0$

\- see [25] for method of determining device parameters

TABLE 4.1 TYPICAL TRANSISTOR PARAMETERS FOR EXP. 4.1, 4.2A, AND 4.2B

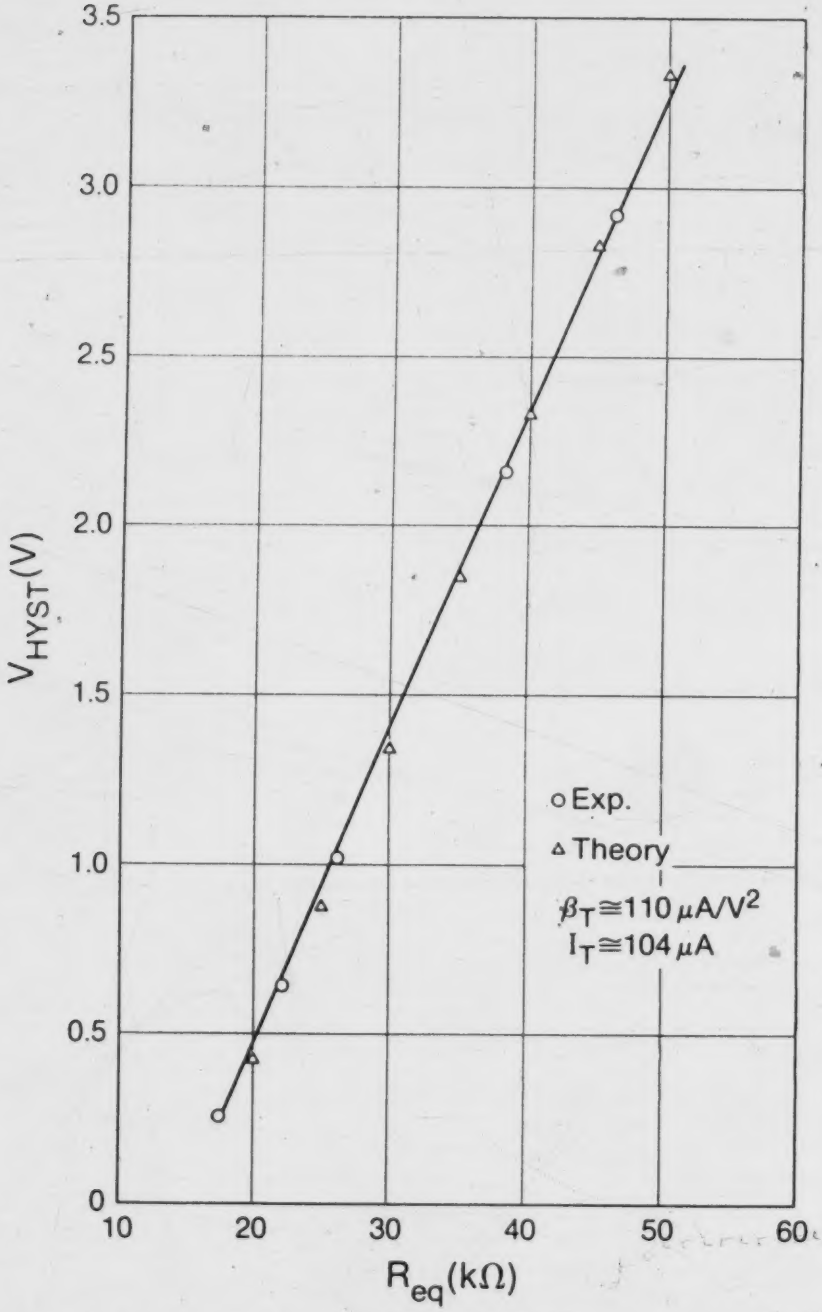


**Figure 4.10 Hysteresis Voltage vs. Threshold Setting Resistance**

of the threshold circuit is understood.

The entire multivibrator was now constructed (Fig. 4.1 and Table 4.2) and the frequency was measured as a function of current $I_C$, with $I_C$ varied from 10 to 100 $\mu$A (one decade). The lower limit for the current is set by the level which could be accurately measured using the available test equipment (about 10$\mu$A), and the upper limit by (from 4.19)

$$I_C \leq I_T \frac{\beta_{nC}}{\beta_{nT}} \tag{4.34}$$

which limits $I_C$ to about 100 $\mu$A maximum since $\beta_{nC} \approx \beta_{nT}$ and $I_T \approx 104$ $\mu$A. Two values of timing capacitor $C$ were used: 220 nF (Exp. 4.2a) and 8.2nF (Exp. 4.2b).

The frequency versus $I_C$ characteristic with the large (220 nF) timing capacitor is shown in Fig. 4.11 along with the predicted values (from 4.21). Within reasonable error the theoretical and experimental results correspond and show a linear relationship between frequency and current, as expected. If the experiment is repeated with the smaller timing capacitor (8.2 nF) and therefore a higher overall frequency range, the frequency versus current characteristic becomes nonlinear (Fig.4.11). Since only the capacitor was changed, the nonlinearity must be a result of switching delays (see 3.1). The total switching delay of the circuit was measured to be about 30 $\mu$S. Subtracting this delay from the frequency characteristic shown in Fig. 4.11 returns it to a straight line.

When the switching delays are insignificant, as for the case of

| | EXP. # 4.2a | EXP. # 4.2b |
|---|---|---|
| $R_1$ (kΩ) | 47 | 47 |
| $R_2$ (kΩ) | 47 | 47 |
| $V_{CC}$ (V) | 10 | 10 |
| C (nF) | 220 | 8.2 |

TABLE 4.2 CIRCUIT PARAMETERS FOR EXP. 4.2A, 4.3B

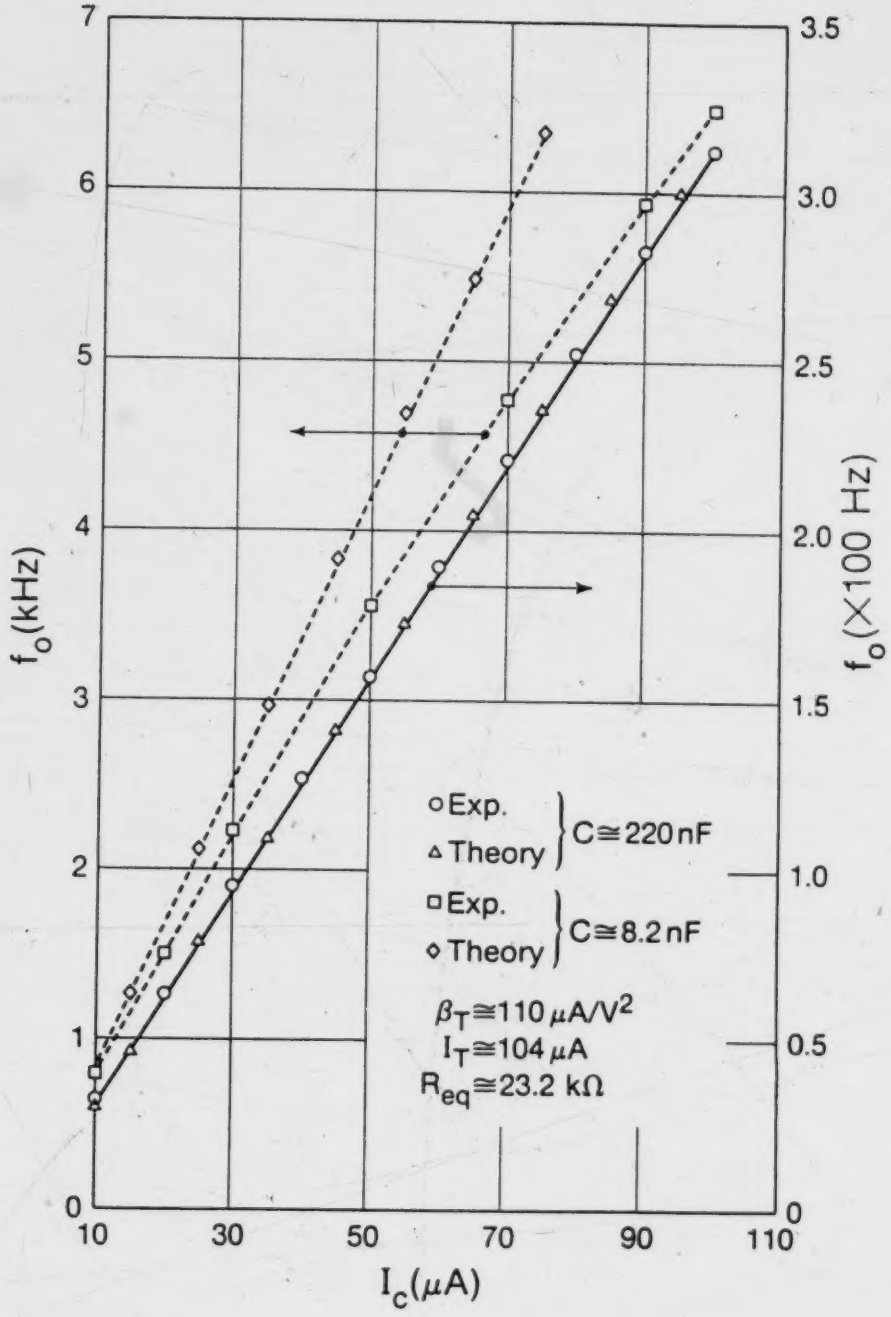


**Figure 4.11 Frequency vs. Control Current for Basic Piskarev Multivibrator**

$C$ = 220 nF, the frequency characteristic can be accurately predicted. Once switching delays become significant compared to the period, the frequency characteristic becomes nonlinear. Integrating the multivibrator should reduce the parasitic capacitances and, therefore the switching delays, considerably.

### 4.8.2 SPICE Simulation: Experiments 4.3a, 4.3b, 4.4

Breadboarding is a suitable investigative tool only at low frequencies. To investigate the Piskarev multivibrator at higher frequencies the circuit's operation was simulated using SPICE [28]. SPICE simulation provides a window on the performance that can expected once the circuit is integrated.

In the basic Piskarev multivibrator the range of frequency control is limited by $I_T$ and $\beta_{nT}$ of the threshold circuit. As discussed in Section 4.7.2 an increased range of frequency control can be obtained by using a buffer stage to drive the charge steering differential pair. Additional switching delays are expected due to the addition of the buffer stage in the signal path. SPICE simulation will be used to investigate the significance of this delay.

The circuit under investigation consists of the basic multivibrator with the addition of a buffer stage (Fig. 4.5). Two connections for the charge steering differential pair will be studied: (1) the gate of M5 is connected to the gate of M2, which is the standard configuration (Fig. 4.5) and will be used as a benchmark (Exp. 4.3a), and (2) the gate of M5 is connected to the output of the buffer (drain of M17) (Exp. 4.3b) to provide additional frequency control range (Fig. 4.6). The input file for SPICE for these

simulations are found in appendix 1.

The two configurations were simulated over a current range of $I_C$ from 10 to 100 μA. The range of control current was set by the limitations (see Sect. 4.4) of the benchmark configuration; the behaviour of the other configuration over a larger current range will be addressed later. For these simulations the timing capacitor was set to 10 pF , a value which is suitable for realization in intergrated form. The results, Fig. 4.12, indicate that the use of the buffer stage to drive the charge steering circuit increases the nonlinearity of the frequency versus current characteristic, due to the increased switching delays. The benchmark configuration had a frequency range of about 0.7 → 3.4 MHz, while the buffered configuration had a range of about 0.7 → 2.5 MHz. Both versions have nonlinear frequency characteristics due to switching delays, but what is significant is that the maximum frequency of the buffered configuration has been reduced by about 25 % due to the additional delays of the buffer stage. At the low end of the frequency characteristic the two configurations are approximately equal. Therefore, the use of the buffer to extend the frequency control range degrades the frequency characteristic near the upper limits, but the penalty at lower frequencies is not as significant. For example, for this set of circuit parameters, if the maximum frequency is kept below ≈ 1 MHz the use of the buffer to increase the control range does not introduce a significant delay penalty.

The above results indicate that for frequencies below approximately 1 MHz the use of the buffer stage to drive the current

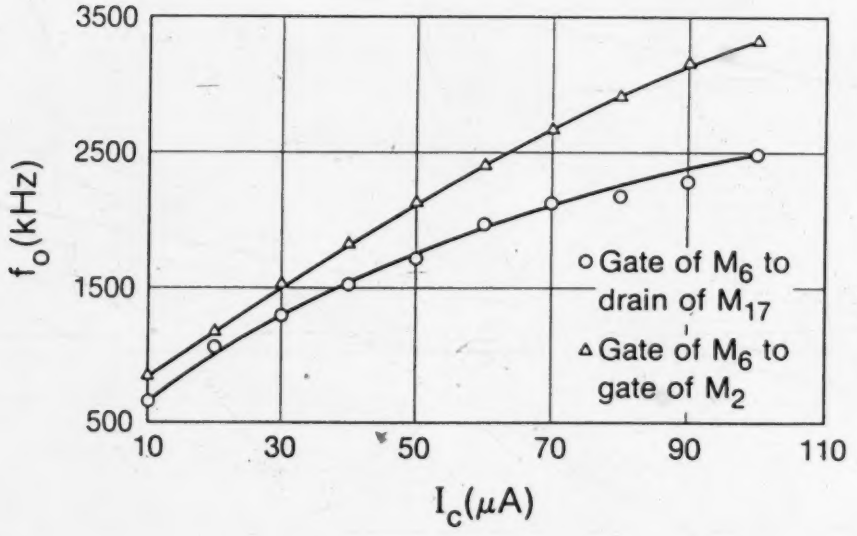


Figure 4.12 Effect of Using Buffer Stage to Control the Charge Steering Circuit

steering stage does not introduce significant additional delays. Using the same extended control range configuration (Fig. 4.6) as before, but with a larger timing capacitor (1 nF) to decrease to maximum frequency, the frequency was measured over a current range of $I_C$ from 3 to 1000 $\mu$A (Exp. 4.4). At current levels much below $\approx$ 3 $\mu$A the charge/discharge currents become asymmetric and the oscillator loses its 50% duty cycle. The results (Fig. 4.13) indicate that frequency control is obtained over the entire range, but switching delays are still significant resulting in a nonlinear frequency characteristic.

## 4.9 Discussion

At low frequencies where the switching delays constitute only a small part of the total period, the hysteresis voltage (4.12) and frequency of oscillation (4.21) can be predicted with good accuracy. As the portion of the period consumed by the switching delay increases, the effective hysteresis voltage grows (due to overshoot) and the frequency versus charge current characteristic becomes nonlinear. At high frequencies, the assumption that at the threshold point the charge current's direction is instantaneously changed, is no longer valid. The delay between the time the capacitor voltage reaches the threshold point and time at which the direction of the charge current is reversed causes the voltage of the capacitor to overshoot the threshold voltage by an amount proportional to the delay. This results in an increase in the effective hysteresis voltage and the subsequent decrease in the oscillation frequency.

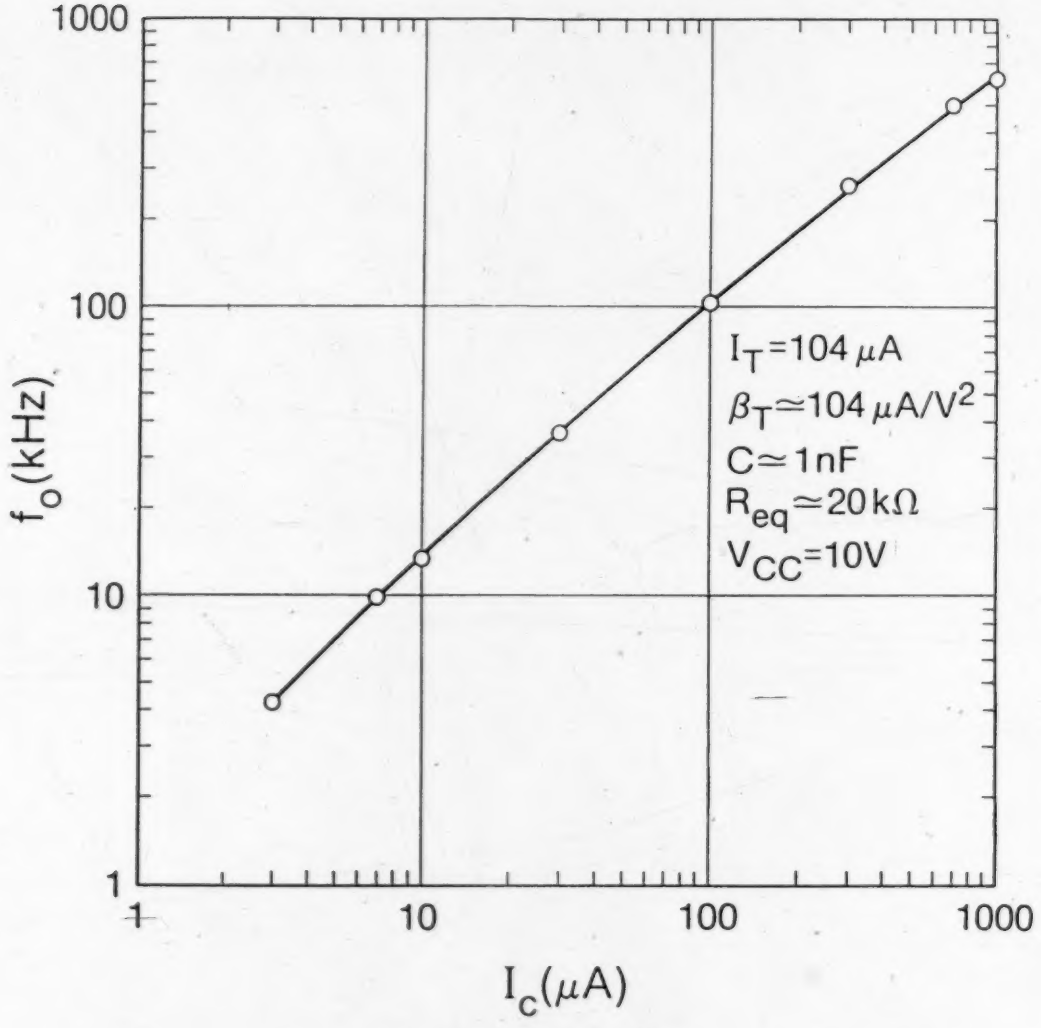


**Figure 4.13 Frequency Characteristic with Extended Control Range**

A wider range of frequency control can be obtained by using the extended control range configuration (Fig. 4.6) as compared to the basic configuration (Fig. 4,5), but the maximum frequency of oscillation will be decreased due to the additional switching delays introduced by the buffer stage. Therefore a tradeoff of the range of control with maximum frequency must be made in choosing between the extended control range and basic configurations.

To reduce the susceptibility of the hysteresis voltage to process and temperature variation the contribution of the term $I_T / \beta_{nT}$ to the overall hysteresis voltage (4.12) should be minimized. This can be accomplished by reducing $I_T$ (limited by the stability of the bias circuitry) and increasing $\beta_{nT}$ (limited by chip area), while maintaining a constant swing at $V_r$ (Fig. 4.1). To maintain a constant swing at $V_r$ the reduction in $I_T$ can be countered by the combination of increasing $R_{eq}$ and the use of current mirror gain (Sect 4.7.4). Ideally the voltage swing at $V_r$ should be large to minimize the influence of $\beta_{nT}$ on the hysteresis voltage and to reduce jitter. The maximum level for $V_r$ is set by either the requirement that M4 remains in pinch off operation (i.e. $V_{CC} - V_{r,high} > | V_{GS,M4} - V_{tp}|$) or speed limitations imposed by the increased delay of large swings. The latter limitation is best tested via SPICE simulations.

Once the term $I_T / \beta_{nT}$ is minimized as described above, further improvements in thermal and process stability of the hysteresis voltage can be made by generating the threshold current in the

appropriate manner. Consider, for example, that:

$$I_T = V_{REF} / R_{bias} \tag{4.35}$$

where

$$R_{bias} = \frac{1}{N} R_{eq} \tag{4.36}$$

and $V_{REF}$ is generated from a thermally stable voltage reference such as a bandgap voltage reference [34]. Now, if $I_T / \beta_{nT} \ll I_T R_{eq}$ and $m_{th} \ll 1$ then the effective hystersis voltage becomes

$$V_{HYST} \approx N V_{REF} \tag{4.32}$$

which is independent to the first order of $R_{eq}$, $\beta_{nT}$, and $I_T$ and only dependent on the thermal and process sensitivity of the reference voltage. For the basic Piskarev multivibrator, the frequency control range is proportional to $I_T/\beta_{nT}$ (4.21); therefore, the reduction of this term in order to decrease the sensitivity of the hysteresis voltage to temperature and process variations occurs at the cost of reduced control range. If a large control range is required and the cost of a reduced maximum frequency is acceptable, the use of the buffer stage to drive the current steering circuit can be used to increase the control range. The buffer stage should be used in most applications, whether or not it is used to drive the current steering stage, to provide conditioning and load driving capability for the output signal.

## 4.10 Conclusion

At low frequencies the operation of the Piskarev multivibrator is well understood and it shows good promise as a simple CCO with good linearity and range of control. A variety of modifications are suggested that allow fine tuning of the circuit's performance for specific applications. As the frequency increases, switching delays cause the frequency control characteristic to become nonlinear. A better understanding of the sources of the switching delays is required. It is uncertain at this point whether the poor performance of the Piskarev multivibrator in terms of switching delays is inherent in its structure and therefore a fundamental limitation, or whether appropriate choice of the transistor dimensions etc., will lead to improved high frequency performance.

## 5.0 Review of Results

### 5.1 Summary of Results

The source coupled and Piskarev multivibrators have not performed as well as was hoped, especially in terms of the frequency control characteristic linearity. The multivibrators, do however, perform as predicted by theory. The behaviour of the multivibrators is understood and the cause of the nonlinearity is known. For the source coupled multivibrator the nonlinearity of the frequency characteristic results from mismatches of the load and threshold device $\beta$'s. This is a fundamental flaw resulting from the structure. The nonlinearity in the frequency characteristic of the Piskarev multivibrator is caused by switching delays. The exact source of the delays is unknown and requires further research, until which point it cannot be ascertained whether or not the delays are fundamental to the structure or can be reduced via careful design.

The primary achievement of this thesis lies not in the performance of the source coupled and Piskarev multivibrators but in the ability to understand and accurately predict their behaviour. An important part of the work is the approach used to find the hystersis voltage of the threshold circuit. The accurate determination of the switching points of the threshold circuit is crucial to accurate frequency calculation. The general approach taken is to use small signal analysis to find the currents in the threshold circuit at the onset of regenerative switching, then use large signal analysis to find the threshold voltage. A variety of other approaches have been proposed [30,31,32,33] for the determination of the hysteresis voltage

of a simple Schmitt trigger (which is what the threshold circuit is). The method proposed here, however, provides a simple and intuitive method which is widely applicable as evidenced by its successful application to the rather different topologies of the source coupled and Piskarev multivibrators.

For CCO applications where linearity is not of prime importance both the source coupled and Piskarev multivibrators are worthy of consideration. The principal advantage of the source coupled multivibrator is its extremely simple and thus compact structure. The Piskarev multivibrator is capable of operating over a wide range of frequencies (almost three decades in the SPICE simulation) and has the advantage of separate charge steering and threshold circuits which is benefical both in terms of linearity and ease of control, at the cost of a slight increase in circuit complexity.

## 5.2 Further Research

The nonlinearity of the Piskarev multivibrator is a result of the switching delays, the source of these delays is uncertain and needs further investigation. It is unknown whether the large delays are fundamental to the structure or can be be reduced through careful design. The major source of the delay is suspected to be parasitic capacitance located at the gate of M2. This capacitance has limited charge/discharge currents, so significant delays may still result even though careful attention was paid to minimizing the voltage swings at this point. The delay at this point is critical since it affects the speed with which the circuit undergoes regenerative switching. Due to

the highly nonlinear nature of the threshold circuit, analysis of the switching delays is a nontrivial problem.

The use of NMOS transitors for both the load and threshold devices of the source coupled multivibrator should be investigated. This will require the circuit to be fabricated in a p-well CMOS technology to allow the NMOS devices to be placed in separate wells so that the body effect can be removed. This is important since any body effect will result in mismatch of the $\beta$'s. By using all NMOS devices the multivibrator should be capable of increased frequency performance (since no slow PMOS devices are used) as well as improved linearity of frequency control due to better matching of the $\beta$'s.

**References**


[1] F.M. Gardner, *Phaselock Techniques*, 2nd ed. New York: John Wiley, 1979.

[2] H.P. Baltes and R.S. Popovic, "Intergrated semiconductor magnetic field sensors," *Proc. IEEE*, vol. 74, no. 8, pp. 1107-1132, Aug. 1986.

[3] S. Middelhoek, P.J. French, J.H. Huising, and W.J. Lian, "Sensors with digital frequency output," *Proc. 4th Int. Conf. Solid-State Sensors and Actuators*,1987, pp. 17-24.

[4] K.D. Wise, "Integrated sensors: key to future VLSI systems," *Proc. 6th Sensor Symp.*,', 1986, pp.1-9.

[5] A.F. Arbel, *Analog Signal Processing and Instrumentation*, Cambridge, Cambridge University Press, 1980.

[6] E. Habekotte, B. Hoefflinger, H.W. Klien, and M.A. Beunder, "State of the art in anlaog CMOS circuit design," *Proc. IEEE*, vol. 75, no. 6, pp. 816-828, Jun. 1987.

[7] J. Mavor, M.A. Jack, and P.B. Denyer, *Introduction to MOS LSI Design*, London: Addision-Wesley, 1983.

[8] Y. Tsividis and P. Antognetti, editors, *Design of MOS VLSI Circuits for Telecommunications*, New Jersey: Prentice Hall, 1985.

[9] A.B. Grebene, *Bipolar and MOS Analog Integrated Circuit Design*, New Jersey: John Wiley,1984.

[10] R.R. Cordel and G. Garrett, "A highly stable VCO for application in monolithic phase-locked loops," *IEEE J. Solid-State Circuits*, vol. SC-10, no. 6, pp. 480-485, Dec. 1975.

[11] J.F. Kukielka and R.G. Meyer, "A high frequency temperature stable monolithic VCO," *IEEE J. Solid-State Circuits*, vol. SC-16, no. 6, pp. 639-647, Dec. 1981.

[12] M.H Wakayama and A.A. Abidi, "A 30 MHz low-jitter high-linearity CMOS voltage controlled oscillator," *IEEE J. Solid-State Circuits*, vol. SC-22, no. 6, pp. 1074-1081, Dec. 1987.

[13] A. Nathan, I.A. McKay, I.M. Filanovsky, and H.P. Baltes, "Design of a CMOS oscillator with magnetic-field frequency modulation," *IEEE. J. Solid-State Circuits*, vol. SC-21, pp. 230-232, Apr. 1987.

[14] *Analog CMOS Integrated Circuit Design Manual*, Ferranti Interdesign Inc., Scotts Valley, Ca.,1983.

[15] I.M. Filanovsky and I.G. Finvers, "A simple nonsaturated CMOS multivibrator," *IEEE J. Solid-State Circuits*, vol SC-23, no. 1, Feb. 1988.

[16] B. Gilbert, "A versatile monolithic voltage to frequency converter," *IEEE J. Solid-State Circuits*, vol. SC-11, no. 6, pp. 852-864, Dec. 1976.

[17] F.V.J. Sleeckx and W.M.C. Sansen, "A wide-band current controlled oscillator using bipolar-JFET technology," *IEEE J. Solid-State Circuits*, vol. SC-15, no. 5, pp. 875-881, Oct. 1980.

[18] A.A. Abidi and R.G. Meyer, "Noise in relaxation oscillators," *IEEE J. Solid-State Circuits*, vol. SC-18, no. 6, pp. 494-496, Jun. 1987.

[19] A.A. Abidi, "Linearization of voltage controlled oscillators using switched capacitor feedback," *IEEE J. Solid-State Circuits*, vol. SC-22, no. 3, pp. 494-496, Jun. 1987.

[20] RCA CMOS Integrated Circuits Data Book (SSD-250C), 1983.

[21] R.S. Muller and T.I. Kamins, *Device Electronics for Integrated Circuits*, 1st ed. New York: John Wiley, 1977.

[22] C.J.M. Verhoeven, "A new model for regenerative circuits," *Proc. 30th Midwest Symp. Circuits and Systems*, pp. 631-634, Aug. 1987.

[23] Y.P. Tsvidis, *Operation and modeling of the MOS transistor*, New York: McGraw-Hill, 1987.

[24] I.M. Filanovsky and V.A. Piskarev, "A simple nonsaturated multivibrator for low voltage power supply," *Int. J. Electronics*, vol. 63, no. 5, pp. 757-765, 1987.

[25] P.E. Allen and D.R. Holberg, *CMOS Analog Circuit Design*, New York: Holt, Rinehart and Winston, 1987.

[26] A. Ambrozy, *Electronic Noise*, New York: McGraw-Hill, 1982.

[27] C. Mead and L. Conway, *Introduction to VLSI systems*, Reading, Massachusetts: Addision-Wesley, 1980.

[28] L.W. Nagel and D.O. Pederson, "Simulation program with integrated circuit emphasis," *Proc. 16th Midwest Symp. Circuit Theory*, April 12, 1973.

[29] *Guide to the integrated circuit implementation services of the Canadian Microelectronics Corporation*, Carruthers Hall, Queen's University, Kingston, Canada, Jan. 1987.

[30] C.J.F. Ridders, "Accurate determination of threshold voltage levels of a Schmitt Trigger," *IEEE Trans. Circuits Syst.*, vol. CAS-32, no. 9, pp. 969-970, Sept. 1985.

[31] S.C.D. Roy, "Comment of accurate determination of threshold voltage levels of a Schmitt Trigger," *IEEE Trans. Circuits Syst.*, Vol. CAS-33, no. 7, pp. 734-735, Jul. 1986.

[32] H.V. Lauer, "Comment on accurate determination of voltage levels of a Schmitt Trigger," *IEEE Trans. Circuits Syst.*, vol. CAS-34, no. 10, pp. 1252-1253, Oct. 1987.

[33] M.J.S. Smith, "On the circuit analysis of the Schmitt Trigger," *IEEE J. Solid-State Circuits*, vol SC-23, no. 1, Feb. 1988.

[34] P.R. Gray and R.G. Meyer, *Analysis and Design of Analog Integrated Circuits*, 2nd ed. New York: John Wiley, 1984.

**List of Related Papers by Author**

I.G. Finvers and I.M. Filanovsky, "Analysis of a source coupled CMOS multibrator," *IEEE Trans. Circuits Syst.*, accepted for publication.

I.M. Filanovsky and I.G. Finvers, "Analysis of a source coupled MOS multivibrator with resistive drain loads," *Int. J. Electronics*, accepted for publication.

I.M. Filanovsky and I.G. Finvers, "A simple nonsaturated CMOS multivibrator," *IEEE J. Solid-State Cicuits*, vol. SC-23, no. 1, Feb. 1988.

**Conference Papers**

I.M. Filanovsky, I.G. Finvers, L. Ristic, and H.P. Baltes, "Multivibrators with frequency control for application in integrated sensors," 1*st Int. Forum ASIC and Transducer Technology*, Feb. 7-10, 1983.

**Appendix 1 SPICE Input Files**

```
Experiment 4.3(a) Piskarev Multivibrator
*    Basic Piskarev Multivibrator with buffer stage, control
*    of current steering stage provided by gate of M2 (see Fig.4.5)
*
.WIDTH  IN=80 OUT=80
.OPTIONS  ABSTOL=1P VNTOL=1U CPTIME=3000 NUMGET=4
+LIMPTS=2000 ITL5=10000
*
*    TRANSISTOR MODELS (FROM [29])
*
.MODEL NTNMOS (LEVEL=2 VTO=1.0
+KP=30.5E-6 GAMMA=1.4 CGSO=4.0E-12
+CGDO=4.0E-12 CGBO=2.0E-12 RSH=15.0
+CJ=4.0E-8 MJ=2.0 CJSW=8.0E-12
+MJSW=2 JS=1E-10 TOX=8.5=-10
+NSUB=1E16 XJ=1E-6 LD=.7E-6
+UO=750 UCRIT=5E4 UEXP=0.14
+VMAX=5E6)
*
.MODEL NTPMOS (LEVEL=2 VTO=-1.0
+KP=10.2E-6 GAMMA=0.635 CGSO=4.0E-12
+CGDO=4.0E-12 CGBO=2.0E-12 RSH=75.0
+CJ=1.8E-8 MJ=2.0 CJSW=6.0E-12
+MJSW=2 JS=1E-10 TOX=8.5=-10
+NSUB=2E15 XJ=0.9E-6 LD=.6E-6
+UO=250 UCRIT=1E4 UEXP=0.03
+VMAX=3E6)
*
*
*    CIRCUIT DESCRIPTION (REFER TO FIG. 4.5)
*
*
M1 12 3 5 5 NTNMOS W=100U L=10U AS=1900P AD=1200P
M2 6 4 5 5 NTNMOS W=100U L=10U AS=1900P AD=1200P
M3 6 6 1 1 NTPMOS W=300U L=10U AS=5700P AD=3600P
M4 4 6 1 1 NTPMOS W=300U L=10U AS=5700P AD=3600P
M5 3 3 2 0 NTNMOS W=150U L=10U AS=2850P AD=1800P
M6 9 11 2 0 NTNMOS W=150U L=10U AS=2850P AD=1800P
M7 3 9 1 1 NTPMOS W=300U L=10U AS=5700P AD=3600P
M8 9 9 1 1 NTPMOS W=300U L=10U AS=5700P AD=3600P
M9 5 7 0 0 NTNMOS W=100U L=10U AS=1900P AD=1200P
M10 7 7 0 0 NTNMOS W=100U L=10U AS=1900P AD=1200P
M11 2 8 0 0 NTNMOS W=100U L=10U AS=1900P AD=1200P
M12 8 8 0 0 NTNMOS W=100U L=10U AS=1900P AD=1200P
M13 12 12 1 1 NTPMOS W=300U L=10U AS=5700P AD=3600P
M14 10 12 1 1 NTPMOS W=100U L=10U AS=5700P AD=3600P
M15 10 10 0 0 NTNMOS W=100U L=10U AS=1900P AD=1200P
M16 11 6 1 1 NTPMOS W=300U L=10U AS=5700P AD=3600P
M17 11 10 0 NTNMOS W=100U L=10U AS=1900P AD=1200P
```

```
*
*
*    THRESHOLD SETTING RESISTORS
*
R1 1 4 40K
R2 4 0 40K
*
*
*    TIMING CAPACITOR
*
C 3 0 10P
*
*
*    CHARGE CURRENT
*
IC 1 8 (CONTROL CURRENT)
*
*
*    THRESHOLD CURRENT
*
IT 1 7 (THRESHOLD CURRNENT)
*
*
*    POWER SUPPLY VOLTAGE
*
VCC 1 0 DC 10
*
*
*    TRANSCIENT ANALYSIS
*
*    SET INITIAL CONDITIONS ON CAPACITOR
*
.IC V(3)=0
*
*    PERFORM TRANSCIENT ANALYSIS
*
.TRAN STEP STOP START UIC
*
*    PLOT THE RESULTS
*    WHERE V(3) IS THE VOLTAGE ON THE TIMING CAPACITOR
*    AND V(11) IS THE OUTPUT OF THE BUFFER STAGE
*
.PLOT TRAN V(3) V(11)
*
.END
```

```
Experiment 4.3(b) Piskarev Multivibrator
*    Basic Piskarev Multivibrator with buffer stage, control
*    of current steering stage (gate of M6) is provided by
*    output of buffer stage (drain of M17) see Fig. 4.6

*
.WIDTH  IN=80 OUT=80
.OPTIONS  ABSTOL=1P VNTOL=1U CPTIME=3000 NUMGET=4
+LIMPTS=2000 ITL5=10000
*
*    TRANSISTOR MODELS (FROM [29])
*
.MODEL NTNMOS (LEVEL=2 VTO=1.0
+KP=30.5E-6 GAMMA=1.4 CGSO=4.0E-12
+CGDO=4.0E-12 CGBO=2.0E-12 RSH=15.0
+CJ=4.0E-8 MJ=2.0 CJSW=8.0E-12
+MJSW=2 JS=1E-10 TOX=8.5=-10
+NSUB=1E16 XJ=1E-6 LD=.7E-6
+UO=750 UCRIT=5E4 UEXP=0.14
+VMAX=5E6)
*
.MODEL NTPMOS (LEVEL=2 VTO=-1.0
+KP=10.2E-6 GAMMA=0.635 CGSO=4.0E-12
+CGDO=4.0E-12 CGBO=2.0E-12 RSH=75.0
+CJ=1.8E-8 MJ=2.0 CJSW=6.0E-12
+MJSW=2 JS=1E-10 TOX=8.5=-10
+NSUB=2E15 XJ=0.9E-6 LD=.6E-6
+UO=250 UCRIT=1E4 UEXP=0.03
+VMAX=3E6)
*
*
*    CIRCUIT DESCRIPTION (REFER TO FIG. 4.5)
*
*
M1 12 3 5 5 NTNMOS W=100U L=10U AS=1900P AD=1200P
M2 6 11 5 5 NTNMOS W=100U L=10U AS=1900P AD=1200P
M3 6 6 1 1 NTPMOS W=300U L=10U AS=5700P AD=3600P
M4 4 6 1 1 NTPMOS W=300U L=10U AS=5700P AD=3600P
M5 3 3 2 0 NTNMOS W=150U L=10U AS=2850P AD=1800P
M6 9 11 2 0 NTNMOS W=150U L=10U AS=2850P AD=1800P
M7 3 9 1 1 NTPMOS W=300U L=10U AS=5700P AD=3600P
M8 9 9 1 1 NTPMOS W=300U L=10U AS=5700P AD=3600P
M9 5 7 0 0 NTNMOS W=100U L=10U AS=1900P AD=1200P
M10 7 7 0 0 NTNMOS W=100U L=10U AS=1900P AD=1200P
M11 2 8 0 0 NTNMOS W=100U L=10U AS=1900P AD=1200P
M12 8 8 0 0 NTNMOS W=100U L=10U AS=1900P AD=1200P
M13 12 12 1 1 NTPMOS W=300U L=10U AS=5700P AD=3600P
M14 10 12 1 1 NTPMOS W=100U L=10U AS=5700P AD=3600P
M15 10 10 0 0 NTNMOS W=100U L=10U AS=1900P AD=1200P
M16 11 6 1 1 NTPMOS W=300U L=10U AS=5700P AD=3600P
M17 11 10 0 NTNMOS W=100U L=10U AS=1900P AD=1200P
*
```

```
*
*    THRESHOLD SETTING RESISTORS
*
R1 1 4 40K
R2 4 0 40K
*
*
*    TIMING CAPACITOR
*
C 3 0 10P
*
*
*    CHARGE CURRENT
*
IC 1 8 (CONTROL CURRENT)
*
*
*    THRESHOLD CURRENT
*
IT 1 7 (THRESHOLD CURRNENT)
*
*
*    POWER SUPPLY VOLTAGE
*
VCC 1 0 DC 10
*
*
*    TRANSCIENT ANALYSIS
*
*    SET INITIAL CONDITIONS ON CAPACITOR
*
.IC V(3)=0
*
*    PERFORM TRANSCIENT ANALYSIS
*
.TRAN STEP STOP START UIC
*
*    PLOT THE RESULTS
*    WHERE V(3) IS THE VOLTAGE ON THE TIMING CAPACITOR
*    AND V(11) IS THE OUTPUT OF THE BUFFER STAGE
*
.PLOT TRAN V(3) V(11)
*
.END
```

```
Experiment 4.4 Piskarev Multivibrator
*    Basic Piskarev Multivibrator with buffer stage, control
*    of current steering stage (gate of M6) is provided by
*    output of buffer stage (drain of M17) see Fig. 4.6
*    Extended control range i.e. I_C is varied from 3 to 1000 μA
*    and C is increased to 10nF
*
.WIDTH  IN=80 OUT=80
.OPTIONS  ABSTOL=1P VNTOL=1U CPTIME=3000 NUMGET=4
+LIMPTS=2000 ITL5=10000
*
*    TRANSISTOR MODELS (FROM [29])
*
.MODEL NTNMOS (LEVEL=2 VTO=1.0
+KP=30.5E-6 GAMMA=1.4 CGSO=4.0E-12
+CGDO=4.0E-12 CGBO=2.0E-12 RSH=15.0
+CJ=4.0E-8 MJ=2.0 CJSW=8.0E-12
+MJSW=2 JS=1E-10 TOX=8.5=-10
+NSUB=1E16 XJ=1E-6 LD=.7E-6
+UO=750 UCRIT=5E4 UEXP=0.14
+VMAX=5E6)
*
.MODEL NTPMOS (LEVEL=2 VTO=-1.0
+KP=10.2E-6 GAMMA=0.635 CGSO=4.0E-12
+CGDO=4.0E-12 CGBO=2.0E-12 RSH=75.0
+CJ=1.8E-8 MJ=2.0 CJSW=6.0E-12
+MJSW=2 JS=1E-10 TOX=8.5=-10
+NSUB=2E15 XJ=0.9E-6 LD=.6E-6
+UO=250 UCRIT=1E4 UEXP=0.03
+VMAX=3E6)
*
*
*    CIRCUIT DESCRIPTION (REFER TO FIC. 4.6)
*
*
M1 12 3 5 5 NTNMOS W=100U L=10U AS=1900P AD=1200P
M2 6 11 5 5 NTNMOS W=100U L=10U AS=1900P AD=1200P
M3 6 6 1 1 NTPMOS W=300U L=10U AS=5700P AD=3600P
M4 4 6 1 1 NTPMOS W=300U L=10U AS=5700P AD=3600P
M5 3 3 2 0 NTNMOS W=150U L=10U AS=2850P AD=1800P
M6 9 11 2 0 NTNMOS W=150U L=10U AS=2850P AD=1800P
M7 3 9 1 1 NTPMOS W=300U L=10U AS=5700P AD=3600P
M8 9 9 1 1 NTPMOS W=300U L=10U AS=5700P AD=3600P
M9 5 7 0 0 NTNMOS W=100U L=10U AS=1900P AD=1200P
M10 7 7 0 0 NTNMOS W=100U L=10U AS=1900P AD=1200P
M11 2 8 0 0 NTNMOS W=100U L=10U AS=1900P AD=1200P
M12 8 8 0 0 NTNMOS W=100U L=10U AS=1900P AD=1200P
M13 12 12 1 1 NTPMOS W=300U L=10U AS=5700P AD=3600P
M14 10 12 1 1 NTPMOS W=100U L=10U AS=5700P AD=3600P
M15 10 10 0 0 NTNMOS W=100U L=10U AS=1900P AD=1200P
M16 11 6 1 1 NTPMOS W=300U L=10U AS=5700P AD=3600P
```

```
M17 11 10 0 NTNMOS W=100U L=10U AS=1900P AD=1200P
*
*
*    THRESHOLD SETTING RESISTORS
*
R1 1 4 40K
R2 4 0 40K
*
*
*    TIMING CAPACITOR
*
C 3 0 10N
*
*
*    CHARGE CURRENT
*
IC 1 8 (CONTROL CURRENT)
*
*
*    THRESHOLD CURRENT
*
IT 1 7 (THRESHOLD CURRNENT)
*
*
*    POWER SUPPLY VOLTAGE
*
VCC 1 0 DC 10
*
*
*    TRANSCIENT ANALYSIS
*
*    SET INITIAL CONDITIONS ON CAPACITOR
*
.IC V(3)=0
*
*    PERFORM TRANSCIENT ANALYSIS
*
.TRAN STEP STOP START UIC
*
*    PLOT THE RESULTS
*    WHERE V(3) IS THE VOLTAGE ON THE TIMING CAPACITOR
*    AND V(11) IS THE OUTPUT OF THE BUFFER STAGE
*
.PLOT TRAN V(3) V(11)
*
.END
```

Appendix 2

Circuits Submitted to CMC for Fabrication

Circuit # 1 Basic Paskarev: see figure 4.1(a)

| DEVICE (REFER TO FIG. 4.1) | W/L |
|---|---|
| 1,2,9,10 | 100/10 |
| 5,6,11,12 | 200/10 |
| 3,4 | 300/10 |
| 7,8 | 600/10 |

TABLE A.1 DEVICE SIZES FOR CMC.1

NOTE: (1) $R_1$,$R_2$,C are external
(2) M1, M2 have no body effect
(3) M5, M6 have body effect
(4) $I_T$,$I_C$ set externally

**Circuit # 2 Basic Piskarev with current mirror gain (3)**

| DEVICE (REFER TO FIG. 4.1) | W/L |
|---|---|
| 1,2,9,10 | 100/10 |
| 5,6,11,12 | 200/10 |
| 3 | 300/10 |
| 4 | 900/10 |
| 7,8 | 600/10 |

TABLE A.2 DEVICE SIZES FOR CMC.2

NOTE: (1) $R_1$,$R_2$,C are external
(2) M1, M2 have no body effect
(3) M5, M6 have body effect
(4) $I_T$,$I_C$ set externally

Circuit # 3 Piskarev Multivibrator with Buffer Stage (see fig. 4.5)

| DEVICE (REFER TO FIG. 4.6) | W/L |
|---|---|
| 1,2,9,10 | 100/10 |
| 5,6,11,12 | 200/10 |
| 3,4 | 300/10 |
| 7,8 | 600/10 |
| 13,14 | 300/10 |
| 15 | 100/10 |
| 16 | 600/10 |
| 17 | 200/10 |

TABLE A.3 DEVICE SIZES FOR CMC.3

NOTE: (1) $R_1$,$R_2$,C are external
(2) M1, M2 have no body effect
(3) M5, M6 have body effect
(4) $I_T$,$I_C$ set externally